© 2023. Published by The Company of Biologists Ltd | Journal of Cell Science (2023) 136, jcs261843. doi:10.1242/jcs.261843

CORRECTION

Correction: Exploring cell and tissue mechanics with optical tweezers

Frederic Català-Castro, Erik Schäffer and Michael Krieg

There was an error in *J. Cell Sci.* (2022) **135**, jcs259355 (doi:10.1242/jcs.259355).

The images in Fig. 1E,F show inverted orange and blue colours for the G′ (storage) and G′′ (loss) labels. The journal apologises to the authors and readers for this error, which occurred during production of the figure.

The corrected and original figure panels are shown below.

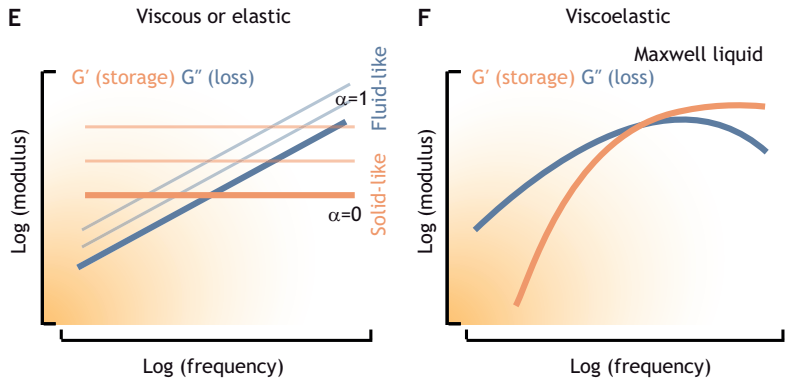

Fig. 1E,F (corrected panels). Measuring and understanding cell mechanics with optical tweezer force curves. (E) Rheological spectrum of a viscous or elastic material. Probing the strain response of a material as a function of frequency provides information about the storage (G′, elastic contribution) and loss (G″, viscous contribution) moduli. In a log–log plot, the slope is equal to the power-law exponent α, indicative for viscous or elastic behavior, while the pre-factor scales with the magnitude of the material property. A change in prefactor leads to a shift along the *y*-axis, without affecting the slope, indicating a change in modulus. See Staunton et al., 2019 for the outcome of a typical experiment. (F) Spectrum of a viscoelastic (Maxwell) material. For low frequencies, loss dominates, as a Maxwell material cannot sustain stress, it flows. A typical example can be found in Jawerth et al., 2020.

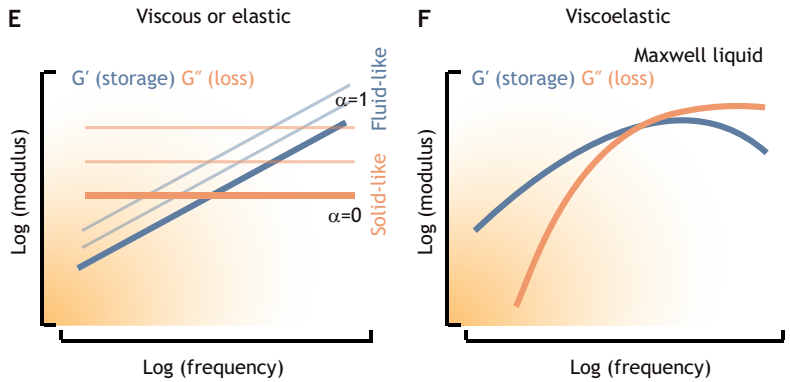

Fig. 1E,F (original panels). Measuring and understanding cell mechanics with optical tweezer force curves. (E) Rheological spectrum of a viscous or elastic material. Probing the strain response of a material as a function of frequency provides information about the storage (G′, elastic contribution) and loss (G″, viscous contribution) moduli. In a log–log plot, the slope is equal to the power-law exponent α, indicative for viscous or elastic behavior, while the pre-factor scales with the magnitude of the material property. A change in prefactor leads to a shift along the *y*-axis, without affecting the slope, indicating a change in modulus. See Staunton et al., 2019 for the outcome of a typical experiment. (F) Spectrum of a viscoelastic (Maxwell) material. For low frequencies, loss dominates, as a Maxwell material cannot sustain stress, it flows. A typical example can be found in Jawerth et al., 2020.

This figure has been corrected in the online and PDF versions of the paper.

© 2022. Published by The Company of Biologists Ltd | Journal of Cell Science (2022) 135, jcs259355. doi:10.1242/jcs.259355

REVIEW

SUBJECT COLLECTION: TOOLS IN CELL BIOLOGY

Exploring cell and tissue mechanics with optical tweezers

Frederic Català-Castro[1], Erik Schäffer[2] and Michael Krieg[1,*]

ABSTRACT

Cellular and tissue biosystems emerge from the assembly of their constituent molecules and obtain a set of specific material properties. To measure these properties and understand how they influence cellular function is a central goal of mechanobiology. From a bottoms-up, physics or engineering point-of-view, such systems are a composition of basic mechanical elements. However, the sheer number and dynamic complexity of them, including active molecular machines and their emergent properties, makes it currently intractable to calculate how biosystems respond to forces. Because many diseases result from an aberrant mechanotransduction, it is thus essential to measure this response. Recent advances in the technology of optical tweezers have broadened their scope from single-molecule applications to measurements inside complex cellular environments, even within tissues and animals. Here, we summarize the basic optical trapping principles, implementations and calibration procedures that enable force measurements using optical tweezers directly inside cells of living animals, in combination with complementary techniques. We review their versatility to manipulate subcellular organelles and measure cellular frequency-dependent mechanics in the piconewton force range from microseconds to hours. As an outlook, we address future challenges to fully unlock the potential of optical tweezers for mechanobiology.

KEY WORDS: Cell mechanics, Forces, Mechanobiology, Optical tweezer, Rheology

Introduction

Robert Hooke coined the term ‘cell’ in 1665 and formulated his famous law of proportionality between stress and strain in 1678. We now know that all animals, plants and fungi consist of these discrete units, the cells. However, their response to mechanical stress is more complicated than Hooke’s law. Cells are composed of molecular complexes that are constantly turned over, reshaped and regulated by active processes that sustain life. The mechanics of these complexes, their interactions and activity provide cells with unique material properties that allow them to resist and transmit mechanical information. But what are these properties?

The cell is a heterogeneous, asymmetric, anisotropic and active medium (Charras et al., 2005; Efremov et al., 2019; Latorre et al., 2018; Turlier et al., 2016), for which no unified theory exists (Dumont and Prakash, 2014). Consequently, we need to broaden our views of cell mechanics away from continuum mechanics and advocate that mechanical properties need to be measured and characterized inside cells with spatial and temporal control. However, only a few techniques allow the measurement of subcellular mechanics non-invasively, for instance with three-dimensional (3D) degrees of freedom to apply strains and compressive, tensile and shear forces over a broad force and frequency range that matches molecular and cellular processes (Roca-Cusachs et al., 2017; Wu et al., 2018).

Here, we review the recent advancement in optical trapping technology, which allows force measurements with piconewton resolution and mechanical manipulations with nanometer precision directly in living cells, organs, and animals. Importantly, to visualize how manipulations affect cell behavior, these measurements can be combined with optical microscopy and other complementary techniques. We discuss relevant challenges and pitfalls and how they can be controlled to unlock the full potential of *in vivo* optical trapping.

Multimodal optical traps to measure and manipulate cellular mechanics inside cells

Art (Arthur) Ashkin invented optical tweezers and first succeeded to trap and manipulate live cells (Ashkin and Dziedzic, 1987; Ashkin et al., 1986, 1987; see also the Nobel Lecture 2018 at https://www.youtube.com/watch?v=vb58pd2ycKQ). To form an optical trap for biological applications, a near infrared laser is focused into or near a cell using a high numerical aperture (NA) microscope objective (Box 1, left-hand side of figure; for detailed descriptions see, for example, Bustamante et al., 2021; Gieseler et al., 2021; Mahamdeh et al., 2011; Neuman and Block, 2004). Near the focus, transparent particles – often microspheres with a diameter of ∼0.5–1.5 µm – can be held by the light as it transfers its momentum, an optical force, onto the particle. These optical forces are proportional to small displacements of the trapped particle, independent of direction so that optical tweezers are 3D Hookean springs. For example, for the x-direction, the force is $F=kx$, where k is the spring constant, the so-called trap stiffness. Although the trap stiffness scales with laser power and depends on direction (Bormuth et al., 2008), typical values for a trap stiffness are 0.1–1.0 pN/nm. With Hooke’s law being valid up to ≈100 nm (Box 1, right-hand side of figure), forces up to 100 pN can be exerted or measured and higher forces up to the escape force can be measured beyond the linear regime (Box 1, 2) (Farré et al., 2017). Robust calibration techniques now enable reliable force and displacement measurements inside cells (for details see Box 2). Furthermore, optical tweezers can be combined with a wide range of imaging or other force-measurement techniques, allowing researchers to obtain complementary, multimodal data to determine the mechanical properties of cells.

Mapping cellular mechanics using optical tweezers

The cellular response to force typically depends on the amplitude, force profile, history, and frequency or duration of the stimulation. Various modalities of optical tweezers have been established to probe and map the mechanical properties of cells (Fig. 1). To extract the stiffness of a sample, a trapped microsphere is driven into a region of interest with a constant speed defining a force ramp (Han et al., 2018; Venturini et al., 2020; Falleroni et al., 2018). The probe is retracted when a user-defined setpoint force or displacement from the trap

[1]Neurophotonics and Mechanical Systems Biology, ICFO, Institut de Ciències Fotòniques, 08860 Castelldefels, Spain. [2]Cellular Nanoscience, ZMBP, University of Tübingen, 72076 Tübingen, Germany.

*Author for correspondence (michael.krieg@icfo.eu)

M.K., 0000-0003-0501-5036

Journal of Cell Science (2022) 135, jcs259355. doi:10.1242/jcs.259355

Glossary

Back-focal-plane interferometry: a position-sensitive device (PSD) or quadrant photo diode placed in a conjugate plane to the back-focal plane of the collecting lens. Because of the location, only displacements of trapped objects relative to the trap center are detected. Thus, independently of the optical trap position in the sample, forces and relative displacements can be accurately measured. Such detectors are primarily force sensors: the readout is directly proportional to force. Using back-focal-plane interferometry, forces and displacements can be measured in 3D.

Catch, slip and ideal bonds: description of an intermolecular interaction whose survival time increases, decreases or is invariant of an applied force. Many structural bonds in the cytoskeleton and during cell adhesion behave as catch bonds, thus, reinforcing force transmission under load.

Complex *G modulus:** measure of the dynamic mechanical properties of a material taking the dissipated energy during deformation and recovery into account. It is equal to the sum of the elastic or storage modulus G' of a material and its viscous or loss modulus G''. During an oscillatory stress, the oscillatory strain follows with a frequency-dependent time lag and amplitude. The complex shear modulus describes the overall resistance to deformation of a material, including recoverable (elastic) and non-recoverable (viscous) deformations.

Entropic spring: unstructured polymer, acting as a spring with a spring constant proportional to temperature. The restoring force on an entropic spring is solely determined by the reduction of its degrees of freedom, i.e. its number of conformations. Only for small extensions, i.e. for a small, non-zero end-to-end distance, is the force applied to an entropic spring proportional to the displacement of the force probe. For larger extensions, the entropic spring stiffens.

Power-law materials: materials with a frequency-dependent modulus $G^*(\omega)$ that can be described by a power law $G^*(\omega)=A\,(i\omega)^{\alpha}$. The scaling factor A describes the magnitude while the exponent α describes the type of response. A higher scaling factor makes a material stiffer or more viscous, whereas a higher exponent makes a material more fluidlike (dissipative).

Power-spectral density: the distribution of total power, derived from a time series measurement of the position of a trapped object, into frequency components. The squared Fourier transform of positional information is calculated and plotted versus frequency; for pure Brownian motion, this analysis yields a typical Lorentzian-like response with a roll-off frequency or corner frequency f_c related to the response time $\tau=1/(2\pi f_c)$. The frequency content is related to the strength of the trap or the mechanics of the surrounding medium.

Relaxation time (material): in an exponential decay, $\sigma(t)=\sigma_0 e^{-t/\tau}$, the decay time, τ, is defined as the time the system needs to relax by a factor of $1/e$. In viscoelastic materials, which respond to strain with elastic and viscous forces, the stress relaxation time is $\tau=\eta/\kappa$, with the stiffness, κ (Pa), and viscosity, η (Pa·s).

Response time (trap): for trapped objects, the response time is given by the ratio of the drag coefficient γ to the trap stiffness, $\tau=\gamma/k$, and is proportional to the object size. For a 1-µm diameter sphere in an aqueous buffer and a trap stiffness of 0.5 pN/nm, the response time is ≈20 µs, corresponding to a corner frequency (see power-spectral density analysis) of about 8.5 kHz. Inside a cell, the response time is increased by the ratio of the cytoplasmic viscosity relative to that of water.

Rheology: branch of material science that studies the flow of matter that cannot be described by a single-viscosity coefficient (non-Newtonian fluids). Applied to cell biophysics, it allows the explanation of how the plasma membrane responds to tension, or how stress is distributed across the cytoplasm during the cell cycle.

Shear modulus *G*: describes response to a shear stress and is related to the Young's modulus by $G=E/[2(1+\nu)]\approx E/3$ for incompressible materials, where ν is the Poisson ratio.

Strain ε: normalized deformation (dimension-less parameter) that an object undergoes upon stress.

Stress σ: amount of force per unit area in units of pressure (Pa) exerted onto an object.

Tensile strength or yield force: maximum stress at which the material breaks or unfolds, and hence stops responding as a linear Hookean spring.

Viscoelasticity: ability of materials to exhibit viscous and elastic properties simultaneously, i.e. to withstand stress only partially.

Viscosity: magnitude of internal friction in a fluid, as measured by the force per unit area resisting uniform flow for a given shear rate. For non-Newtonian fluids, it depends on the shear rate, i.e. the velocity of the force probe. The viscosity of water is 1 mPa·s at 20°C; that of the cytoplasm ranges from 1–50 mPa s.

Young's modulus *E*: ratio between the applied stress and the resulting strain induced on an elastic object by extension, so that $\sigma=E\varepsilon$. It is a material property with units of pressure (Pa) that does not depend on object shape or size. The higher the Young's modulus, the stiffer the elastic material is. The Young's modulus is typically measured by atomic force microscopy (AFM) and ranges from 100 Pa for brain tissue to 10,000 Pa for muscle or even higher for bone.

center is reached (Fig. 1A). In this manner, a force–deformation curve is recorded. Imaging of large cell deformations by spinning disk confocal (Català-Castro et al., 2021) or light-sheet microscopy (Chardès et al., 2018) aids the real-time analysis of force-induced cell shape changes. Depending on the mechanical behavior of the biosystem, either a certain continuum model can be used to obtain quantitative information, or model-independent parameters need to be extracted to compare different experimental conditions. In general, a larger slope in the force–deformation curve indicates a higher sample stiffness and, thus, readily provides insight into structural strength of force transmission (Han et al., 2018, 2020) and mechanical resistance of the cytoplasm (Hu et al., 2017). The same approach can be used to measure a viscoelastic response, for example, by driving the trap with increasing velocities into the structure of interest.

If the optical trap is equipped with a force-feedback system (Bugiel et al., 2017), the force can be clamped to a user-defined setpoint (Lang et al., 2002) and duration while the resulting probe displacement is recorded (Fig. 1B). After the response time and assuming a linear-elastic (Hookean) solid that is probed with a constant area, the strain is directly proportional to the stress (see Glossary), with the proportionality constant being the Young's modulus (see Glossary) of the sample (Fig. 1B). In a purely viscous (Newtonian) fluid (see Glossary), a constant stress results in a continuous flow of the material. Without restoring forces, the initial position will not be recovered once the stress is released and the applied force is set to zero. In a viscoelastic material (see Glossary), a constant stress results in a larger deformation as the material flows and results in a creep compliance curve $J(t)$. To determine the frequency-dependent rheological spectrum (see Glossary), this curve can be transformed (see below). After release of the force at the end of the experiment, the deformed material partially relaxes back towards its starting geometry (Fig. 1B). However, due to energy dissipation, the starting position might not be recovered. The force clamp is also obtained in the so-called optical stretcher – a setup of two counter-propagating laser beams that is frequently used to retrieve the mechanical footprint of non-adherent cells in a high-throughput manner (Ekpenyong et al., 2012; Guck et al., 2005).

Experimentally easier to implement is the trap position clamp (Fig. 1C). Here, the sample is indented to a constant value by a fast movement of the trap to a new position while the resistance and force relaxation is recorded. The relaxation time (see Glossary) can be extracted and provides insight into the viscosity of the sample. Note that the time to relocate the trap needs to be shorter than the relaxation time of the viscous or viscoelastic sample response. The conversion of the force into a stress yields the stress-relaxation curve (Khalilgharibi et al., 2019; Tassieri et al., 2016).

Journal of Cell Science (2022) 135, jcs259355. doi:10.1242/jcs.259355

Box 1. Principle and realization of optical tweezer experiments

Principle

Optical tweezers are force and position transducers. With a trapping lens, a laser, typically with an infrared wavelength and a Gaussian beam profile, is focused onto a sample (left-hand side of figure). In the laser focus, small dielectric objects with a higher refractive index compared to the medium can be trapped and manipulated. Using these probes, active processes or the mechanical properties of cells and their organelles, such as the nucleus, mitochondria, cytoskeleton, Golgi and ER, can be measured. For measurements with a collection lens, the forward scattered light is projected onto a position-sensitive device (PSD) placed in the back focal plane. Based on the deflection of the laser beam, piconewton forces and nanometer displacements can be detected. The force generated inside the cell, for example by a motor (F_{motor}), is equal to the optical trap force (F_{trap}=F_{motor}).

Steering and detection

Often, not only detection, but also fast 3D manipulation of trapped particles is desired and essential. Sample stages allow for relative movement of the trap to the sample. For vertical-position control, stages or a tunable lens are used (Schäffer et al., 2007; Falleroni et al., 2018). For faster lateral control, the laser beam is steered using tilt mirrors (Bugiel et al., 2017; Florin et al., 1997), acousto- and electro-optical deflectors [AODs (Visscher et al., 1996; Vermeulen et al., 2006) and EODs (Valentine et al., 2008; Woody et al., 2018)] or spatial light modulators (Català-Castro and Martín-Badosa, 2021; Dufresne et al., 2001). With AODs, multiple traps can be formed by time sharing the same laser onto different positions (Guilford et al., 2004). During manipulation, the trapped object's displacement is recorded either through particle imaging and tracking (Hörner et al., 2017; Mejean et al., 2009), or with back-focal-plane interferometry (Farré et al., 2012; Gittes and Schmidt, 1998) using either a quadrant photo diode or PSD (Bui et al., 2018; Huisstede et al., 2005; Mahamdeh and Schäffer, 2009) (left-hand side of figure, also see the Glossary). Although PSDs detect the centroid of the light distribution and are advantageous for direct force measurements (Farré and Montes-Usategui, 2010), quadrant photo diodes may provide a higher bandwidth (Berg-Sørensen and Flyvbjerg, 2004; Jannasch et al., 2011). Since both types of detectors record voltages, these signals need to be calibrated (Box 2).

Nonlinear effects

For displacements up to ≈100 nm, the trap stiffness corresponds to the slope of the force–displacement curve (~0.5 pN/nm for the cyan line in the right-hand side of figure). For larger displacements, the trap stiffens for particle diameters larger than ≈0.8 µm (Bormuth et al., 2008), here illustrated for a diameter of 2 µm, until a maximum force, the so-called escape force, is reached. Note that when using direct force measurements to estimate mechanical properties, such as the complex shear modulus, probe displacement needs to be recorded independently. Therefore, measurements need to be performed within the linear detection range, or a separate stationary detection laser can be used to determine the particle position beyond the linear detection range (Neuman and Block, 2004). From a practical point of view, we recommend to choose a trapping-probe size and laser power so that maximum force is reached within the linear detection range (Bormuth et al., 2008; Mahamdeh et al., 2011).

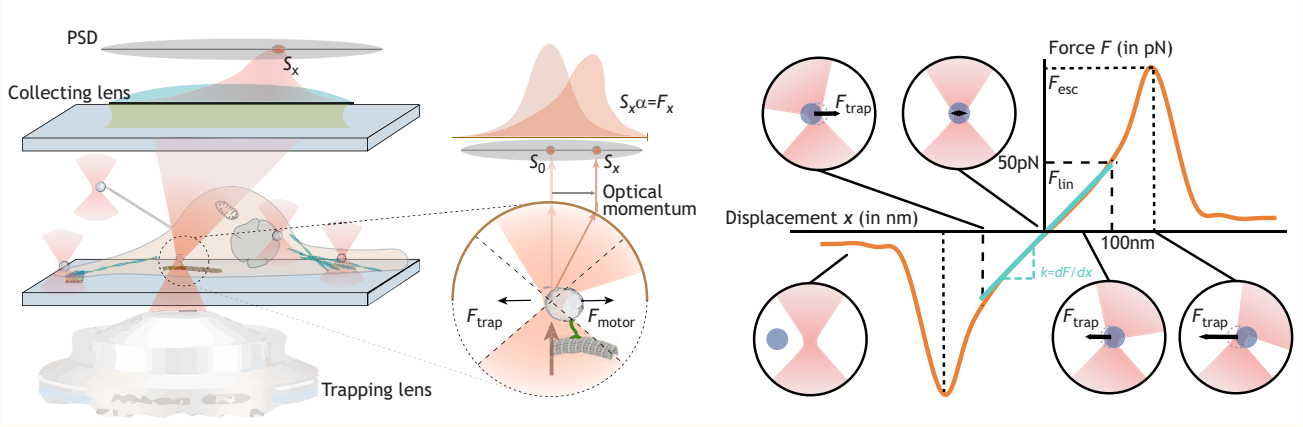

A special implementation of a position clamp is membrane tether extrusion force spectroscopy (Fig. 2A). While recording the force, a lipid membrane nanotube is pulled from the plasma membrane of cells *in vitro* (Das et al., 2021; Datar et al., 2015; Nussenzveig, 2017; Raucher and Sheetz, 2000), or inside living animals (Johansen et al., 2016). The obtained force curves contain rich information about the membrane–cortex interface. The initial formation of the membrane tube is hindered by an energy barrier (Koster et al., 2005) that provides insight into local membrane curvature (Ma and Berro, 2021). The force needed to further extrude the membrane tube provides important information about membrane–cytoskeleton coupling (Sheetz, 2001) and the lipid reservoir (Dai and Sheetz, 1995a; Raucher and Sheetz, 1999), as well as membrane tension, bending rigidity and membrane viscosity (Hochmuth et al., 1996). With higher pulling speeds, forces increase as lipids need to diffuse into the tether, membrane viscosity contributes significantly and proteins accumulate at the tether neck (Tian and Baumgart, 2009). Importantly, once the trap is stationary, the extrusion force relaxes to a constant value (Fig. 2A) that depends on the membrane tension and is largely independent of the pulling history (Dai et al., 1998). Using an appropriate mathematical model, it is possible to relate the force and velocity to the density of attachment points between the membrane and the cytoskeleton (Brochard-Wyart et al., 2006).

Determining the rheological spectrum of a cell

Because the mechanical properties emerge from their constituent parts, every organelle has a distinct rheological spectrum that depends on the measurement frequency (Chen et al., 2010), location and age (Khan et al., 2019; Majumdar et al., 2018). Owing to the small probe size and 3D navigability, optical tweezers can perform spatially resolved measurements to map mechanics within the same cell (Mandal et al., 2016). In an active microrheology experiment, the frequency-dependent viscoelastic properties can be derived from

Journal of Cell Science (2022) 135, jcs259355. doi:10.1242/jcs.259355

Box 2. Calibration

Optical forces on trapped particles and measurement bandwidth depend on particle dimension, shape, composition, its refractive index and that of the medium, incident laser power, wavelength, polarization, mode and angular distribution, temperature, viscosity, distance to nearby surfaces and the trap center, optical aberrations, the detector and data acquisition hardware (Berg-Sørensen and Flyvbjerg, 2004; Bormuth et al., 2008; Mahamdeh et al., 2011; Schäffer et al., 2007). Because trapping parameters are challenging to calculate (Dutra et al., 2014), they are usually measured. For back-focal-plane interferometry, unknown parameters include the drag coefficient of the trapped particle, the displacement sensitivity β (volt-to-nanometer conversion factor in nm/V), the trap stiffness k (pN/nm), or alternatively a force sensitivity α (volt-to-piconewton conversion factor in pN/V) for direct force measurements. To determine these quantities, the system is calibrated against thermal forces, a known applied drag force or displacement, or a combination thereof to minimize assumptions (Tolić-Nørrelykke et al., 2006). Owing to conservation of the momentum of the light, forces can be measured directly by quantifying the angular intensity distribution of light scattered by a trapped particle (Smith et al., 2003). If all photons are collected, the force is directly proportional to the centroid position S_x of a position-sensitive device with the force sensitivity α (see Box 1, inset in left-hand side of figure). This parameter is independent of the experimental details and only needs to be determined once for a given setup (Farré and Montes-Usategui, 2010). Thus, when trapping inside cells, direct force sensing is especially useful, since many parameters that influence optical forces may be unknown. However, for mechanical measurements, not only force but also probe displacements need to be measured. Since no conservation laws are applicable, calibration of displacements is still necessary and more challenging inside cells. One solution may be camera-based position detection as it avoids complicated displacement-sensitivity calibrations, nonlinear effects, and has achieved kilohertz bandwidth (Barak et al., 2013; Huhle et al., 2015).

Since optical tweezers are 3D Hookean springs, force and displacement of the trapped probe are proportional to back-focal-plane-interferometry detector voltages. For example, for the x-direction, the displacement is given by a multiplication with the displacement sensitivity, $x_{probe}=\beta S_x$, and the force by $F=kx=k\beta S_x=\alpha S_x$ (Box 1, inset in left-hand side of figure). Therefore, the force sensitivity $\alpha=k\beta$ is directly related to the trap stiffness and displacement sensitivity, and can be used to calibrate them (Farré et al., 2012). To determine the displacement sensitivity, a known relative displacement of the particle from the trap center or a detection laser is typically used (Neuman and Block, 2004; Tolić-Nørrelykke et al., 2006; Staunton et al., 2017). For a rheological spectrum of a cell, the time resolution is limited by the response time of the trapped probe (see Glossary). In general, the smaller the particle and its drag coefficient, and the higher the trap stiffness, the better the time resolution, which is currently limited to ∼10 µs (Neupane et al., 2016; Sudhakar et al., 2021). Shorter times or corresponding higher frequencies are inaccessible. Together with the roll-off frequency and comparison to thermal forces, the drag coefficient and trap stiffness can be directly measured. In this manner, the trap is fully calibrated without assumptions about the shape or size of the particle, for example, of trapped cellular organelles, or the viscosity of the medium (Schäffer et al., 2007; Tolić-Nørrelykke et al., 2006).

a trapped microsphere that is oscillated at various frequencies with small displacement amplitudes that fall within the linear regime (Box 1) (Guo et al., 2014; Tassieri, 2019). Depending on the mechanical property of the material, the measured force either follows the microsphere position perfectly (purely elastic) or lags behind resulting in a phase difference or lag δ (Fig. 1D). In a purely viscous material, this phase lag is exactly 90° or π/2, meaning that the force is proportional to the speed. In general, for a viscoelastic material, the phase lag has an intermediate value and is recorded for different frequencies, yielding information about the complex shear modulus (see Glossary) of the material (Fig. 2E). The complex shear modulus $G^*(\varpi)= G'(\varpi) + iG''(\varpi)$ at a given angular frequency ϖ has a real and imaginary part that describe the capability of the material to store, i.e. the storage modulus $[G'(\varpi)]$, or dissipate, i.e. the loss modulus $[G''(\varpi)]$, mechanical energy, respectively (Ayala et al., 2016).

The rheological spectrum for viscoelastic materials shows that the shear modulus is not a material constant, as it changes with the strain rate – the modulus strongly depends on the frequency. Thus, the material can be soft at low frequency and impenetrably hard at high frequencies. It is common to use empirical power-law models, for example $G^*(\varpi) = A(i\varpi)^{\alpha}$, to extract information from the measurements. For each modulus, the exponent α can be obtained from the slope of the $G^*(\varpi)$ versus ϖ curve in a double logarithmic plot (Fig. 1E). Its magnitude informs whether liquid ($\alpha\rightarrow1$) or solid ($\alpha\rightarrow0$) properties dominate in the material (Fig. 1E). Intermediate values indicate that the material is viscoelastic. Furthermore, the exponent itself can depend on the frequency (Blehm et al., 2016; Bonfanti et al., 2019; Hurst et al., 2021) (Fig. 1F). In this case, a simple power law is not sufficient to describe the mechanical response, and more sophisticated mechanical models need to be considered (Bonfanti et al., 2020). The lag δ is related to the ratio of the loss over the storage modulus $G''/G' = \tan\delta$, also called the loss tangent. Values larger than one indicate that energy dissipation is dominant corresponding to a more liquid-like behavior. For example, fluidization ($\tan\delta>1$) at higher frequencies might indicate a destabilization of intermolecular bonds under stress (Hurst et al., 2021; Lee et al., 2010). Conversely, stress-stiffening owing to reorientation and entanglement (Khan et al., 2019) or catch-bond kinetics and motor-based prestress of cellular material (Chen et al., 2010; Han et al., 2018) might lead to a frequency dependent loss tangent.

Mapping mechanical properties from the cell surface to the nucleus

Most cells are sufficiently transparent so that stable optical traps can be generated inside the cytoplasm of isolated cells. Unlike atomic force microscopy, which is limited to the cell surface (Krieg et al., 2019), with the cantilever obstructing simultaneous optical access, optical tweezers offer the opportunity to explore individual subcellular compartments directly with minimal mechanical and optical interference of other cellular structures (Fig. 2A–F).

Local plasma membrane mechanics

Much of our understanding of how biological membranes respond mechanically has been derived from the extrusion of lipid tethers (or nanotubes; Fig. 2A) from cells (Dai and Sheetz, 1995b; Hochmuth et al., 1996; for a recent review, see Nussenzveig, 2017). In particular, tether extrusion showed that local differences in plasma membrane tension regulate many cellular processes, including polarized cell migration (Houk et al., 2012; Lieber et al., 2015), stress relieve (Sinha et al., 2011), parasite infection (Kariuki et al., 2020) or phagocytosis (Berghoff et al., 2021; Masters et al., 2013), and exo- and endo-cytosis (Gomis Perez et al., 2022), as well as mechanosensitive ion channel gating (Das et al., 2021). Despite these insights, it is still disputed how stress distributes within the membrane (Cohen and Shi, 2019).

Many cells have a large plasma membrane reservoir, stored as caveolae or other membrane invaginations, that is able to buffer changes in membrane tension (Raucher and Sheetz, 1999; Singh and Lamaze, 2020). However, the existence of such a reservoir is

Journal of Cell Science (2022) 135, jcs259355. doi:10.1242/jcs.259355

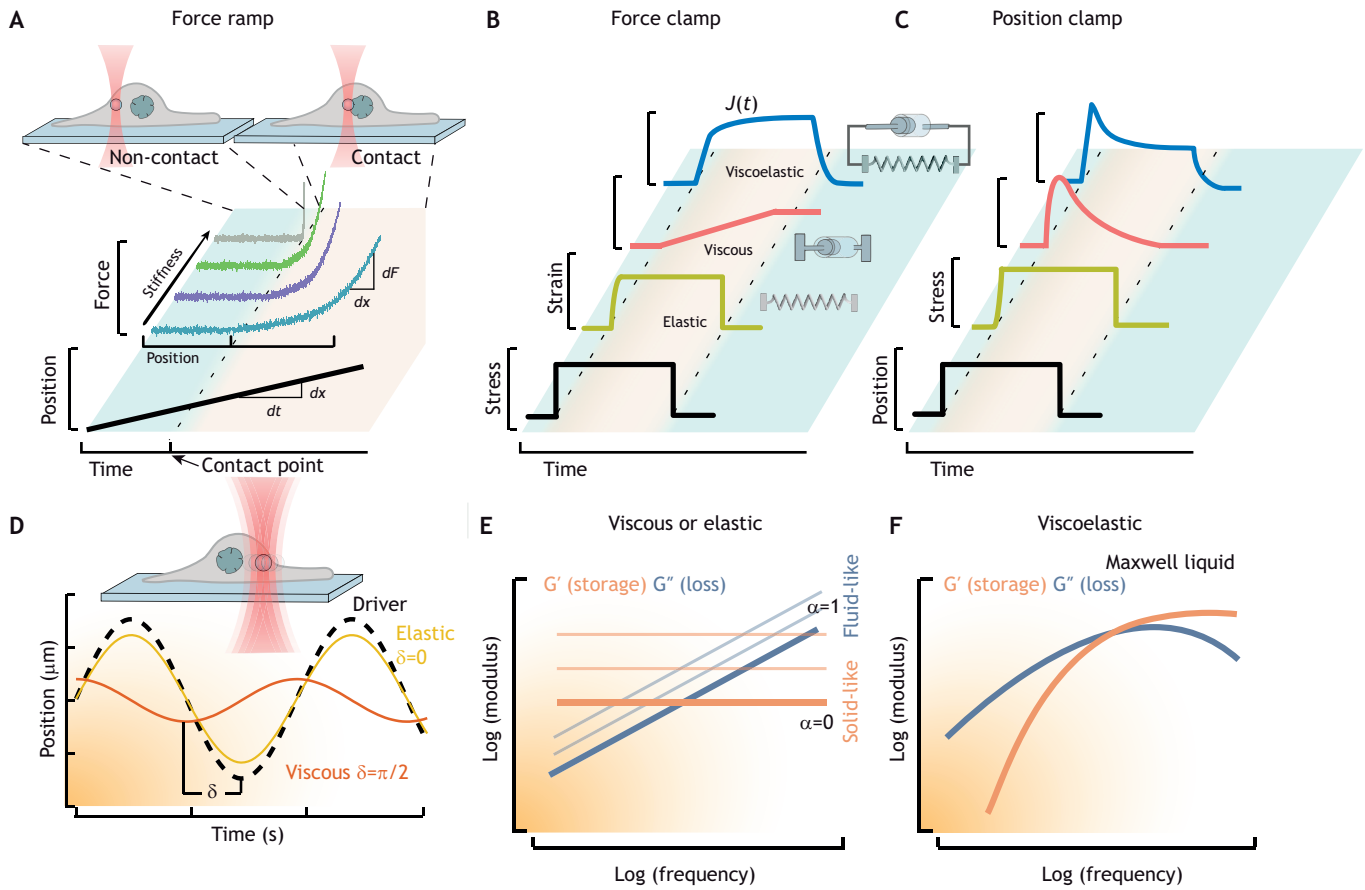

Fig. 1. Measuring and understanding cell mechanics with optical tweezer force curves. (A) Force-ramp indentation experiment. The trapped particle is driven into a cellular structure with a constant trap velocity *dx*/*dt*. Before contact, viscous drag between the microsphere and the cytoplasm or friction on reticular organelles might induce a significant and detectable force before contact with the desired target, for example, the nucleus. The resulting force-indentation curves represent the contact mechanics with the slope *dF*/*dx* (*x*=indentation), which is related to the stiffness κ of the sample by $F=\kappa x$ for a linear elastic material. The different slopes of the curves represent stiffer materials. The dashed line indicates where the microsphere contacts the sample. (B) Force-clamp experiment. A force-feedback system is used to maintain a constant stress on the sample with a predefined contact force (black curve). Typical strain response curves for an elastic (yellow), viscous (red), and viscoelastic material (blue) with a non-linear deformation during contact, called creep compliance *J*(*t*), are shown. To obtain the complex shear modulus, the creep compliance can be transformed to a frequency spectrum (see below). Schematics indicate mechanical elements of a spring and dashpot (damper). (C) Position-clamp experiment. A constant deformation is applied to the cell (black) while recording the stress–relaxation curve. A linear elastic material relaxes back to its equilibrium shape after the stress is released (yellow). A viscous material (red) dissipates the stress, relaxing to zero. An intermediate behavior is seen in viscoelastic materials (blue). (D) Active microrheology. To measure the associated phase lag δ between the force and microsphere position in a viscoelastic material, a microsphere is oscillated with various frequencies. (E) Rheological spectrum of a viscous or elastic material. Probing the strain response of a material as a function of frequency provides information about the storage (G′, elastic contribution) and loss (G″, viscous contribution) moduli. In a log–log plot, the slope is equal to the power-law exponent α, indicative for viscous or elastic behavior, while the pre-factor scales with the magnitude of the material property. A change in prefactor leads to a shift along the *y*-axis, without affecting the slope, indicating a change in modulus. See Staunton et al., 2019 for the outcome of a typical experiment. (F) Spectrum of a viscoelastic (Maxwell) material. For low frequencies, loss dominates, as a Maxwell material cannot sustain stress, it flows. A typical example can be found in Jawerth et al., 2020.

inconsistent with a long-range membrane-based transmission of mechanical stress, as any difference in tension would act as a sink for superfluous membrane. Thus, local alterations in tension are rapidly damped over long distances and could prevent a fast mechanical signaling across the cell surface (Shi et al., 2018).

The combination of optical-tweezer-based tether pulling with multimodal imaging has afforded new insights into the regulation of force-activated ion channels. By exerting forces locally on the membrane, the spatial extent and the direction of the tension gradient can be investigated. High-tension gradients during membrane extrusion reduces the basal Ca^{2+} activity in proprioceptive neurons through activation of K^+ ion channels, whereas membrane tether relaxation caused a strong increase in local Ca^{2+} signaling through activation of TRP ion channels (Das et al., 2021). Such experiments point to mechanically compartmentalized axons that can process multiple stimuli at the same time (Krieg et al., 2022).

Cytoskeleton and motor proteins

Actin, microtubule and intermediate filament networks have all been demonstrated to contribute to cytoplasmic strength, organelle stability and flow in a cell type-specific manner (Guo et al., 2013; Hu et al., 2019; Mandal et al., 2016). Actin-based traction forces inside lamellipodia and filopodia can be measured using optical traps, while simultaneously observing protein dynamics (Leijnse et al., 2014; Mehidi et al., 2021). Indeed, forces during actin dynamics and their coupling to the WAVE regulatory complex (WRC), a complex that links actin to various cell surface receptors (Chen et al., 2014), have recently been mapped in the lamellipodium of cultured cells. By specifically attaching functionalized

Journal of Cell Science (2022) 135, jcs259355. doi:10.1242/jcs.259355

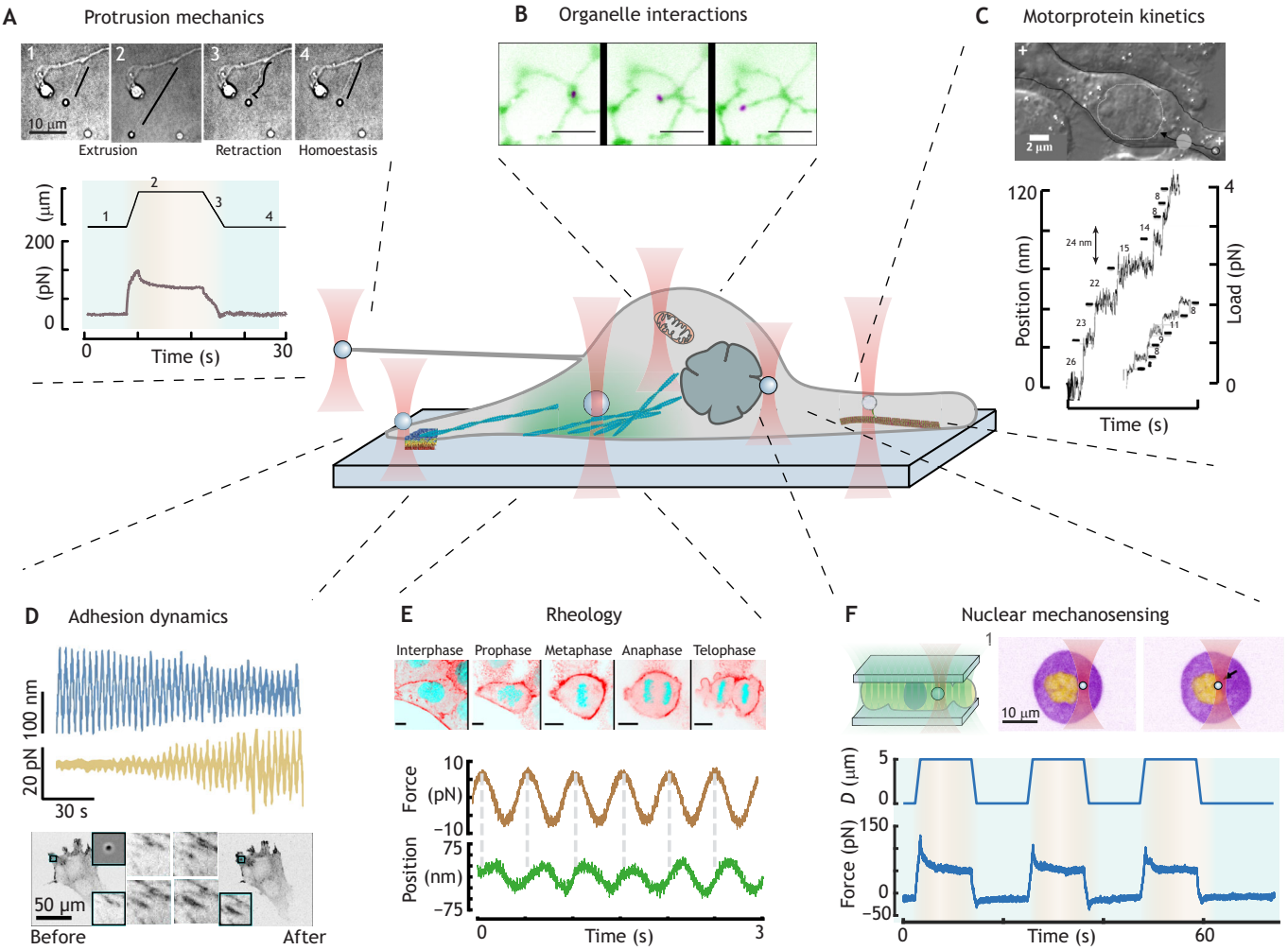

Fig. 2. Optical manipulation and measurement of biological processes inside living cells. (A) Protrusion or membrane mechanics. In a lipid tether extrusion experiment, a microsphere is brought into contact with the membrane and retracted. The membrane tension results in a force directed against the direction of movement and relaxes as the microsphere position is clamped. Numbers in the representative optical micrographs correspond to the position in the force profile below (note tube buckling during retraction). (B) Organelle interactions. Intracellular mechanical manipulation of a trapped mitochondria (purple) that is pulled away from the ER (green) is used to test the hypothesis that Miro2 actively promotes mitochondrial fusion through ER interaction. Reproduced from White et al. (2020), where it was published under a CC-BY 4.0 license. Scale bars: 5 µm. (C) Motor protein kinetics. Image of a cultured cell with phagocytosed microspheres (white). The black trajectory indicates a dynein-powered microsphere that moves towards the minus end of a microtubule and passes through a static optical trap (gray circular area). The plot on the right shows the stepping dynamics of the phagosome under increasing load, resulting in a decrease in step size from 24 to 8 nm. Reproduced with permission from Rai et al. (2013) with permission from Elsevier. (D) Adhesion dynamics. Loading-rate-dependent stiffening probed with fibronectin-labeled microspheres attached to integrins and oscillated with a constant amplitude showing strain-stiffening and strengthening of the integrin adhesion. Blue trace shows the reduction in displacement, yellow the increase in force measured during the history of the experiment. The recruitment of focal adhesion proteins during the stimulation shown in the images underneath led to a force increase. Adapted from Andreu et al. (2021), where it was published under a CC-BY 4.0 license. (E) Rheology. Micrographs of a cell during mitosis with a single embedded microsphere with representative force (beige) and position (green) traces below obtained from an active microrheology routine. The frequency-dependent phase lag indicates a viscoelastic response and, importantly, a softening of the cytoplasm during cell division, suggesting that mechanical properties are regulated and under cellular homeostasis. Reproduced with permission from Springer Nature, Nature Physics (Hurst et al., 2021). Scale bars: 10 µm. (F) Nuclear mechanosensing. To test the mechanosensitive capacity of the nucleus, a trapped microsphere indents the nucleus of a cell under confinement. Two confocal microscopy images of a zebrafish cell before and after indentation of the nucleus. The arrow points to a trapped microsphere. Representative probe position *D* and force relaxation traces during a typical indentation experiment.

microspheres to modified cell surface receptors, bound to the WRC on the intracellular side, the specific interaction strength of the receptor with the cortical actin cytoskeleton during protrusion formation was measured with an optical trap (Mehidi et al., 2021). Forces above 2 pN, close to the polymerization force of individual actin filaments, lead to detachment of the receptor from WRC, suggesting that force on the WRC controls lamellipodium formation and migration (Mehidi et al., 2021).

Optical tweezers have also been used to directly explore force transmission pathways through the actin cytoskeleton. For instance, microspheres functionalized with the actin-binding drug phalloidin have been delivered into cultured cells by microinjection and used as direct handles to pull on actin stress fibers (Hayakawa et al., 2008). To visualize the consequences of this force, intracellular calcium dynamics were simultaneously recorded by total internal reflection fluorescence (TIRF) microscopy in a multimodal setup. A pulling force of 5.5 pN opened mechanosensitive transduction channels close to focal adhesions, suggesting that mechanical stress was directly transmitted through the actin cytoskeleton to activate mechanosensitive ion channels (Hayakawa et al., 2008).

Journal of Cell Science (2022) 135, jcs259355. doi:10.1242/jcs.259355

Because microinjection of microspheres into cells is laborious, force measurements are frequently performed on phagocytosed microspheres (Blehm et al., 2013; Hendricks et al., 2012; Rai et al., 2013) (Fig. 2C), endogenous cellular lipid droplets that bidirectionally move along microtubules (Shubeita et al., 2008; Sims and Xie, 2009) or artificial organelles (López-Quesada et al., 2014), all of which can be trapped easily based on their refractive index mismatch with the surrounding medium. Compared to endogenous vesicles, microspheres have a larger refractive index and enable higher forces. Independently of whether phagocytosed microspheres or lipid vesicles are used to manipulate their motor-driven transport, the stepping forces and kinetics has been shown to be consistent with *in vitro* dynein and kinesin experiments (Fig. 2C) (Rai et al., 2013; Sims and Xie, 2009). Remarkably, it is possible to obtain mechanical information inside cells with single-molecule precision down to forces of 1 pN (Rai et al., 2013). The effect of the collective motor force generation can also be directly measured with active rheology, and the cytoplasm of cancer cells becomes more fluid-like upon inhibition of kinesin motors (Mandal et al., 2019).

The cellular response to forces is determined by the interaction kinetics between the proteins within the force transmission pathway. Because individual interactions can react to force either with an increase or decrease in lifetime (see Box 3), the application of a piconewton force might influence the turnover of proteins in a cellular complex (Novikova and Storm, 2013). Note that based on the rate-dependent kinetics of single-molecule interactions (Merkel et al., 1999), mechanosensitive processes might be more sensitive to certain frequencies but insensitive to others. For example, focal adhesions grow larger if force is applied at a higher frequency, even if the magnitude of the applied force is unchanged (Fig. 2D) (Andreu et al., 2021). To account for this effect, experiments need to be carried out over a large range of frequencies, strain rates or loading rates.

Cytoplasm

The cytoplasm has complex mechanical properties, and it is far from being a homogenous medium. Its spatiotemporal organization depends on membrane-enclosed organelles and phase-separated membrane-less condensates. Even though these condensates await detailed mechanical characterization inside cells, *in vitro* optical tweezers experiments have shown that many of these are viscoelastic materials with a strong frequency-dependent storage and loss modulus (Alshareedah et al., 2021; Ghosh et al., 2021; Jawerth et al., 2018, 2020). Many have been shown to stiffen under mechanical stress (Shen et al., 2020), while others change their relaxation time as they age. This property could have profound consequences on their biochemical functions (Jawerth et al., 2020) and mechanotransduction (Sanfeliu-Cerdán et al., 2022 preprint).

To investigate the local mechanical environment in the vicinity of the probe, embedded microspheres or lipid vesicles can be used as passive force probes (Turlier et al., 2016; Zia, 2018). Here, the optical trap is stationary, and the Brownian and cell-generated motion are detected (Mason and Weitz, 1995; Tassieri, 2019). By a power spectral analysis of the tracked motion, the frequency-dependent response of the surrounding cytoplasm, for example, the power-law behavior of its complex shear modulus, can be obtained. The resulting exponent α is characteristic for the material properties of the viscoelastic medium (α=0 elastic, α=1 viscous, and α>1 active, non-equilibrium material). Often, an exponent of α=0.75 is found, which is characteristic for semi-flexible polymers, such as the actin or extracellular matrix (ECM) network, for example, in the tail and brain of zebrafish (Blehm et al., 2016). This approach has provided insights into the local mechanical properties in cellular protrusions, such as axial tension, bending flexural rigidity and plasma membrane tension (Gárate et al., 2015; Valentino et al., 2016), as well as how cytoplasmic rheology correlates with the migratory cell behavior of cancer organoids (Reuten et al., 2021; Wullkopf et al., 2018), or tissue formation in developing animals (Dzementsei et al., 2022). However, passive microrheology approaches are not valid universally; especially at low frequencies, active energy consumption of the cell increases the mechanical motion of the tracer particles (Guo et al., 2014). This leads to a violation of the fluctuation–dissipation theorem (Turlier et al., 2016), meaning that ATP consumption by motor activity increases the fluctuations compared to those expected at thermal equilibrium. Also, the small, passive amplitudes limit detectable displacements in very rigid environments. Thus, care needs to be taken when interpreting passive microrheology measurements (Mizuno et al., 2008).

Box 3. The mechanical properties of cells arise from their complexity

Modeling

Any mechanical system, including the building blocks and molecular machines of cells, can in principle be described by a composition of passive and active mechanical elements (Bonfanti et al., 2019). Once the force generators are known, then the dynamic response of the system can in principle be calculated. However, most models assume that the material is isotropic, homogenous and linear without a memory of stress history. Because living cells do not fulfil these assumptions, modeling leads to a simplified description of cell mechanics.

Biopolymers

To understand the mechanical response on the (sub-)cellular and tissue level, the dynamic response of the individual components and how they interact with each other needs to be known. Folded proteins have material properties that resemble hard plastics with a Young's modulus of ≈2 GPa and tensile strength of ≈0.1 GPa (see Glossary; Howard 2001). As their yield force is approached, proteins unfold; they do not obey Hooke's law anymore. Many unstructured biopolymers form entropic springs (see Glossary) that might be cross-linked to networks with a nonlinear response to force. Such a response allows a different sensitivity and response under different conditions (Sharma et al., 2021).

Dynamics, protein friction and active processes

Interactions between and within biomolecules are mostly mediated by weak non-covalent bonds that form and break. Their dynamics is important for the overall response of the system. When subjected to force, interactions break as ideal, slip or catch bonds (see Glossary) (Rakshit et al., 2012). Rupture forces and bond lifetimes depend in a complex manner on how force was applied (Evans and Calderwood, 2007). Furthermore, any bond rupture when subjected to force is the molecular origin for dissipation and friction between proteins (Bormuth et al., 2009). In analogy to friction between macroscopic bodies in contact moving relative to each other, a significant amount of friction between proteins exists and adds to the viscous response of the cytoplasm. Since protein friction depends on the shear rate, it contributes to the nonlinear, viscoelastic response of cells. Unbinding and binding of bonds between successive loading trials can cause a history effect, which can lead to strain stiffening or stress softening.

Apart from the binding kinetics, further active dynamic processes contribute to the complexity of cells. For example, the dynamics and regulation of filament length, and the turnover cycles of molecular machines define characteristic time scales for force generation, loading rates and response to external stimuli. Furthermore, growth, biological signaling and feedback lead to an active response on various time scales making the overall stress response a highly nonlinear, local, and time-dependent process. To understand these processes, we need to be able to measure them and optical tweezers provide the most exquisite tool to do so inside cells.

An alternative to passive is active microrheology; this is where a trapped microsphere is actively oscillated while force and displacements are simultaneously recorded (see Fig. 1D above). Active microrheology has led to new insights into the physics of living matter and how energy consumption modifies the viscoelastic response of the cytoplasm (Guo et al., 2014; Mandal et al., 2019) and its mechanical organization (Ahmed et al., 2018; Hu et al., 2017). For example, it has been shown that the cytoplasm fluidizes during cell division (Hurst et al., 2021). Fluidization reduces the drag on chromosomes while they move through the viscous material and facilitates cell division (Fig. 2E). Conversely, the cytoplasm stiffens during water efflux, due in part to an increase in intracellular molecular crowding (Guo et al., 2017).

Nucleus

The nucleus is the biggest cellular organelle and has received much attention in mechanobiology. It is a transducer of mechanical stress and significantly contributes to the mechanical properties of the whole cell (for reviews, see Nader et al., 2021; Niethammer, 2021). Atomic force microscopy, micropipettes and magnetic tweezers have been used, but these methods also deform the cell membrane and cytoplasm. In contrast, optical tweezers can directly probe the nucleus without unwanted activation of cell-membrane-mediated mechanotransduction. For example, the mechanical properties of the nucleus have been shown to be the origin of a proprioceptive signal in response to 3D compression, which triggers early events during confined migration in development (Venturini et al., 2020) (Fig. 2F). It has been found that nuclei deform non-linearly and display rapid viscoelastic relaxations, a property that appears to be unaffected by modest 3D confinement (Català-Castro et al., 2021). How confinement in general affects the rheological response of the nucleus is unknown.

Changes in nuclear mechanics also relate to cancer progression, for example, in the transition from grade III to IV glioma (Alibert et al., 2021). Based on active microrheology measurements of the nucleus, nuclear stiffness increased in grade IV compared to grade III glioma, whereas the bulk cytoplasm and actin cortex softened (Alibert et al., 2021). This counterintuitive result highlights that the mechanical properties of different cellular organelles and compartments might be differentially affected during a physiological or pathological process. Such local changes are difficult to measure by other techniques. Although most of these experiments use spontaneous microsphere internalization, subcellular particles are sometimes also used. For instance, in mouse oocytes, the nucleolus has a different refractive index to the surrounding nucleoplasm. Thus, nucleoli could be trapped and used as a microrheology probe for the nucleolus–chromatin complex (Syrchina et al., 2020). This approach is particularly valuable, as delivery of microspheres into the nucleus is inherently difficult.

In plants, tip growth depends on the nucleus position (Ketelaar et al., 2002). Its manipulation in root cells with optical tweezers stopped growth. Here, nucleus positioning likely did not involve actin bundling, hinting at a novel mechanotransduction pathway between the cell surface and the nucleus (Ketelaar et al., 2002).

Organelle mechanics

Owing to their excellent spatial resolution, optical tweezers offer the possibility to manipulate organelle-organelle interactions, map membrane contact sites and dynamically reposition individual components with respect to one another (Fig. 2B) (Gao et al., 2016; Guet et al., 2014; Kim et al., 2015; Osterrieder et al., 2017). In tobacco leaf epidermal cells, it was recently shown that mitochondria interact with the endoplasmic reticulum (ER), which affects mitochondrial fusion through the small GTPase Miro (White et al., 2020). Furthermore, chloroplasts strongly attach to the ER with forces exceeding 400 pN, presumably reflecting the site of inter-organelle lipid exchange (Andersson et al., 2007). Less is known regarding organelle mechanosensation in mammalian cells. In a pioneering study, locally applied force at the membrane of mesenchymal stem cells activated Ca^{2+} dynamics originating from ER-based ion channels (Kim et al., 2015). Such an activation might be important for stem cell differentiation. Taken together, the versatility of optical-tweezer-based force measurements has afforded unprecedented insight into intracellular mechanics. Future work will help to dissect the contribution of different organelles to cellular mechanotransduction (Feng and Kornmann, 2018).

Measuring mechanics in tissues, animals and plants

In contrast to various other force spectroscopy techniques (Roca-Cusachs et al., 2017; Wu et al., 2018), optical tweezers have the ability to measure and apply forces inside cells of tissues, embryos and moving animals (Fig. 3). In transparent animals, optical tweezers even enable measurements through tissue boundaries, for example, the characterization of complex fluid dynamics of native blood flow (Harlepp et al., 2017).

Therefore, complementary to microscopy methods, optical tweezers enable the characterization of the relationship between structure and mechanics, and how this relationship tunes the force sensitivity of the cellular functions within their respective native environments. For instance, to investigate the forces that control stability and morphodynamics during embryogenesis and record how local deformations propagate throughout the tissue, optical tweezers have been used to deform cell–cell junctions in combination with light microscopy (Fig. 3A) (Bambardekar et al., 2015; Ferro et al., 2020). In these experiments, no microspheres were used, as the cell junction itself could be trapped and deformed by the trapping laser. Creep compliance measurements and the resulting viscoelastic properties of cell junctions have helped to explain morphogenetic events, such as cell intercalations during germ band extension in fruit flies (Bambardekar et al., 2015) or primitive streak formation in chicken embryos (Fig. 3A) (Ferro et al., 2020).

Light-sheet microscopy together with optical tweezers has been used to manipulate mechanically sensitive processes, while measuring behavior and whole-brain Ca^{2+} activity inside living zebrafish (Fig. 3B) (Favre-Bulle et al., 2017, 2018). Like other vertebrates, zebrafish use vestibular otoliths, composed of a gelatinous matrix, in each ear for 3D orientation in their environment. A 5 pN force exerted on the otoliths evoked complex calcium dynamics in the brain and a behavioral response, visible as eye movement and compensatory tail displacement in a restrained zebrafish (Favre-Bulle et al., 2017).

In intact plant tissue, optical tweezers have been used to manipulate organelle–organelle interactions (Fig. 3C) (Leitz et al., 2009). Mechanical deformations of the ER with trapped intracellular statoliths leads to a long-lasting mechanoresponse that affects gravitropism in root cells of *Arabidopsis thaliana*, possibly through gating of ER-resident mechanosensors (Leitz et al., 2009; Sparkes, 2018). The force necessary to reposition and deform other plant organelles are in the lower piconewton range, making optical tweezers, for example, combined with confocal microscopy an ideal tool to investigate gravitropism and other mechanical plant processes (Abe et al., 2020).

During zebrafish development, optical-tweezer-based active and passive microrheology has shown that gut progenitors acquire

Journal of Cell Science (2022) 135, jcs259355. doi:10.1242/jcs.259355

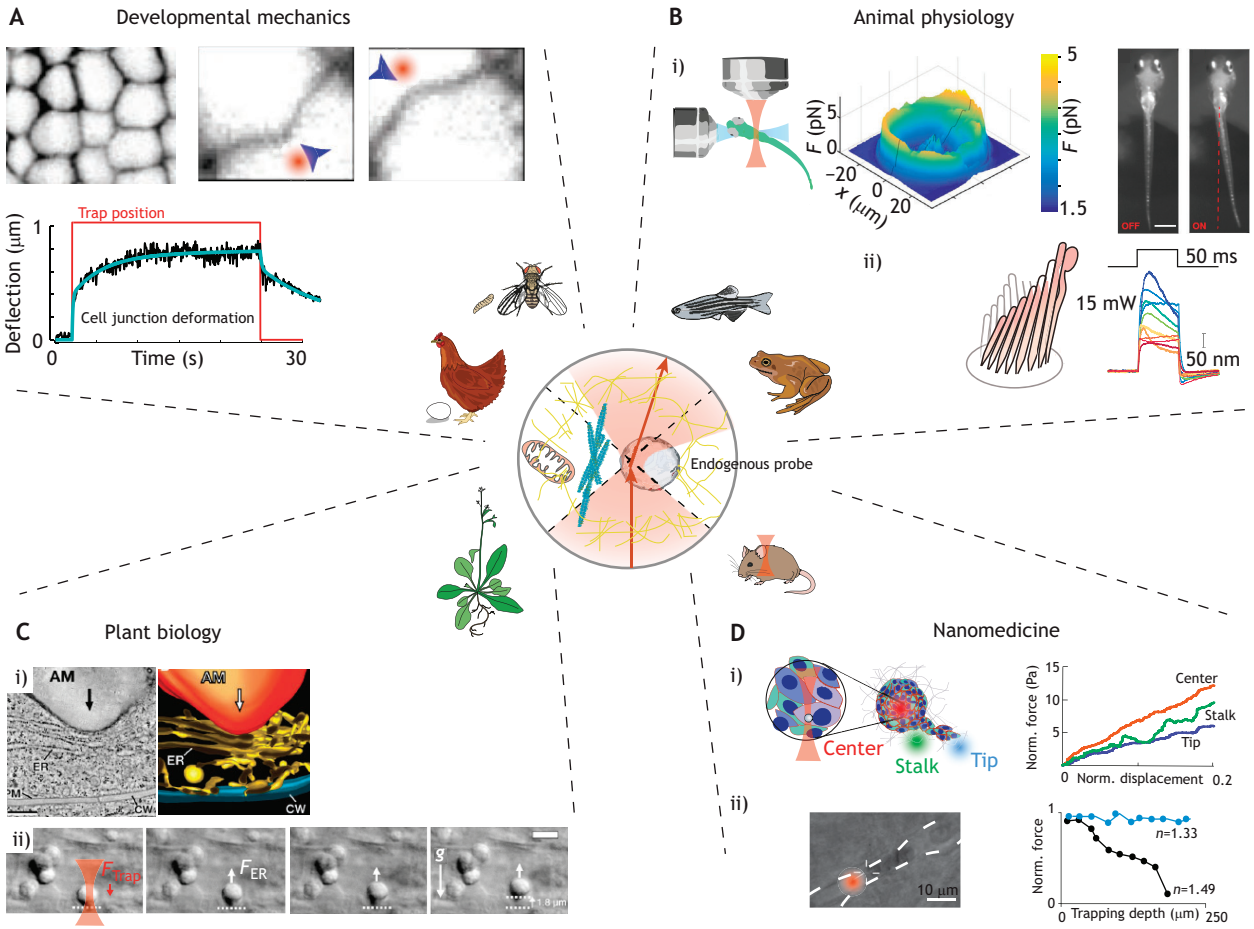

Fig. 3. Subcellular mechanics in intact tissues and animals. (A) Developmental mechanics. Optical tweezers enable assessment of mechanics in complex organisms. Light-sheet micrograph of a *Drosophila* embryonic epithelium and two representative close-ups of a deformed cell–cell junction pointed out by blue arrowheads. The force–time trace shows the junction deformation (black) and trap position (red). Reproduced with permission from Bambardekar et al. (2015). (B) Animal physiology. Specific stimulation of a mechanosensitive structure in the ear of intact zebrafish (i) and explant bullfrog sacculus (ii) enables measurements of piconewton force and nanometer displacements, respectively. (i) Left, schematic of the experiment. Middle, 3D diagram of the force applied to an otolith. Owing to its irregular shape, the force was not constant in all directions. Right: snapshot of a zebrafish larva before and after manipulation of the otolith in its inner ear showing compensatory tail movement upon force application (i.e. deflection to the right). Reproduced from Favre-Bulle et al. (2017), where it was published under a CC-BY 4.0 license. (ii) Schematic of a photonic stimulation experiment, in which a laser deflects the hair bundle of a bullfrog sacculus. 15-mW power caused deflections of several 100 nm providing a powerful method to measure fast biological dynamics. Reproduced from Abeytunge et al. (2021), where it was published under a CC-BY 4.0 license. (C) Plant biology. ER elastic deformation visualized with optically trapped statoliths in intact gravity sensing columnella root cells of *Arabidopsis*. (i) Electron micrograph and its tomogram of a statolith (AM) deforming the cortical ER. (ii) A trapped statolith is pushed against the lower cell wall and elastically rebounds from the cortical regions (dashed line) after the trapping laser is switched off. ***g***, gravitational force; F_{trap}, trapping force, F_{ER}, force due to stored elastic energy in the ER. CW, cell wall. Scale bars: 5 µm. Reproduced from Leitz et al. (2009), where it was published under a CC-BY 4.0 license. (D) Optical tweezers for nanomedicine. (i) Mechanical characterization of cancer cells within their native tissue. Schematic of an MCF10 organoid with a 'stalk' of invading cells leaving the spheroid. Representative force–distance curves derived from subcellular, embedded microspheres in different regions of the metastatic cancer spheroids demonstrate that cells in these regions have distinct mechanical properties related to their invasive potential. Curves with a higher slope in the force–displacement graph reflect cells with higher stiffness. Adapted with permission from Springer Nature, Nature Physics (Han et al., 2020). (ii) Nanosurgical procedure to clear clogged arteries in the earlobe of an immobilized mouse. Optical tweezers were used to remove a jammed red blood cell from the constriction, thus re-establishing blood flow. Plot showing that trapping strength in deep tissues is limited due to optical aberrations induced by refractive index mismatch. Reproduced with permission from Springer Nature, Nature Communications (Zhong et al., 2013).

higher elasticity than their surrounding cells. These changes were attributed to their microtubule cytoskeleton (Dzementsei et al., 2022), while differences between brain and tail vasculature might be due to their specific ECM (Blehm et al., 2016; Staunton et al., 2019). The emergence of certain properties is not restricted to development but also occurs during pathological processes, such as cancer morphogenesis. To understand the mechanical behavior of cancer metastasis, rheology measurements have been carried out in primary tumors (Reuten et al., 2021; Staunton et al., 2016) and cancer spheroids (Han et al., 2020; Wullkopf et al., 2018). In such spheroids, different tissue regions adopt distinct mechanical properties (Fig. 3D) that correlate with their invasive potential (Wullkopf et al., 2018). For example, independently of the cancer type, the invading tip cells displayed a higher scaling exponent α than the cells located in the center of the organoids, suggesting that a higher fluidity correlates with invasiveness (Wullkopf et al., 2018). These experiments support the hypothesis that cells with a higher deformability have a higher propensity to migrate through tissue barriers and confined spaces. Finally, the ability of optical tweezers to perform non-invasive operations with high precision have been exploited in nano-surgical applications. Blood clots have been removed from obstructed arteries of living mammals (Fig. 3D)

(Zhong et al., 2013). These proof-of-principle experiments demonstrate the versatility and power of optical tweezers.

Limitations and future perspectives

Despite the promises optical tweezers hold for intracellular force and displacement measurements, several important points need to be considered when planning, executing and analyzing optical mechanics measurements inside cells and animals (Català-Castro et al., 2021; Pompeu et al., 2021). Those include changes in light momentum due to the refractive index mismatch inside cells, the choice of the probe particle size and its refractive index, laser-induced heating, optical aberrations when working in deep tissue, and the rheological response of active matter.

Refractive index mismatch through cells and tissues

The cytoplasm has a higher refractive index (n_{cyto} is ∼1.38) compared to that of cell culture medium (n_m of ∼1.33, close to that of water) (Schürmann et al., 2016). Thus, the trapping laser is deflected at the cell surface, eventually leading to a change in light momentum. Even though this deflection can be exploited to apply forces to objects in cells without a microsphere, the additional deflection when using microspheres may lead to an underestimation of force. This effect can be noticed when approaching a cell from the outside as an attractive force prior to actually making contact with the cell membrane (Riesenberg et al., 2020). When working with cells *in vitro*, refractive index-matching media could be used to reduce this mismatch (Boothe et al., 2017).

Microsphere size

Even though measurements of light momentum enable calibration-free force measurements on particles of arbitrary size and shape (Bui et al., 2018; Català et al., 2017a), the maximum force is limited by particle size (Bormuth et al., 2008). However, large microspheres are difficult to target directly inside cells, might interfere with biological processes and have a nonlinear force-displacement relation (Box 1, right-hand side of figure). Conversely, inside cells, it is difficult to trap small particles with a diameter much smaller than the trapping wavelength. First, Brownian forces might exceed optical escape forces. Second, when focusing through layers having different refractive indices, aberrations might weaken the trap. Depending on whether a high trap stiffness or a high escape force is desired, the optimal choice of particle size can be different. The highest trap stiffness occurs at the Mie resonance, where the particle size matches the trapping laser wavelength in the medium. Thus, for a 1064-nm laser, a microsphere diameter of 800 nm in water or 770 nm in cytoplasm results in the highest force within the linear optical force regime (Box 1) (Bormuth et al., 2008; Mahamdeh et al., 2011). However, force–displacement relationships are nonlinear when approaching maximal forces (Box 1, right-hand side of figure). Within the linear range, forces can be increased up to 40% based on the choice of laser polarization matching the measurement direction (Bormuth et al., 2008). Thus, depending on the application, different microspheres might be desirable. To guide the range of accessible parameters, several computational optical tweezer toolboxes allow the exploration the degrees of freedom *in silico* (Callegari et al., 2019; Lenton et al., 2017; Nieminen et al., 2007). To aid the investigations of mechanical properties of specific cellular structures, microspheres can be coated with biomolecules. Such functionalized microspheres can then be enriched at actin cables or at cell surface receptors (Hayakawa et al., 2008; Mehidi et al., 2021; Meloty-Kapella et al., 2012).

Force limit

Compared to other manipulation techniques, a major drawback is the low force limit of optical tweezers – usually less than 400 pN for a laser power of <1 W in the laser focus. As a consequence, deformations are small with the benefit that linear elastic regimes of biological materials are probed. Higher forces, or the same forces with less light and photodamage, can be achieved by using cleverly engineered, high-refracting micro- or nano-spheres (Cordova et al., 2018; Ferro et al., 2016; Jannasch et al., 2012; Sudhakar et al., 2021), large microspheres trapped by structured light (Taylor et al., 2015) or off-resonance trapping of upconversion nanoparticles (Shan et al., 2021). Such particles have not yet been used inside cells, but they should be well-suited to apply high forces onto organelles or probe higher frequency regimes in a rheology experiment with lower laser power as compared to a direct manipulation of cellular structures with lower refractive index. Generally, the refractive index of the trapping probe should be as high as possible. For example, microspheres composed of melamine (n=1.68) have a higher trap stiffness than those of polystyrene (n=1.59) having the same size (Català et al., 2017a). However, backscattering of light from microspheres with a very high refractive index limits stable trapping, and antireflective coatings are necessary (Bormuth et al., 2008; Jannasch et al., 2012).

Heating

With increased laser power, sample heating may cause a heat-shock response (Hörner et al., 2017; Leitz et al., 2002) and a decrease in viscosity that might affect calibration (Peterman et al., 2003). Most trapping probes are transparent and heating is mostly due to the absorption of the trapping laser by water (≈10 K/W; Peterman et al., 2003). Metallic particles, however, should be avoided, especially inside cells (Andres-arroyo et al., 2015). Thus, overall heating can be minimized by the choice of the most efficient optical trapping probe and laser wavelength (Català et al., 2017b; Leitz et al., 2002).

Deep-tissue aberrations

Thick or highly curved specimens might deflect the trapping laser due to the cell curvature or an optically dense particle within the optical path. Opaque samples or turbid tissues also limit the penetration depth of the trapping laser (Favre-Bulle et al., 2019). Thus, an important requirement for the use of optical tweezers is the transparency of the sample and optimal optics to generate a stable trap. Stable traps require a high NA lens for focusing. However, high-NA oil immersion lenses introduce spherical aberration when trapping inside aqueous environments, degenerating trap quality (Fig. 3Dii; Zhong et al., 2017). With optimal aberration correction, high-NA water immersion lenses, and index-matching media, deeper trapping beyond 150 µm should be feasible (Dzementsei et al., 2022). Also, wavefront-shaping techniques using adaptive optics can be applied to minimize aberrations due to scattering, and thereby allow better trapping at increased penetration depths (Favre-Bulle et al., 2019).

A complex active mechanical response

The mechanical complexity of biological cells poses a challenge for the interpretation of rheological data (Bonfanti et al., 2020; Verdier, 2003). The non-linear, non-isotropic and history-dependent active response (see Box 3) can be teased apart in force spectra, but care needs to be taken in their evaluation. For example, non-linear visco-plastic effects can be tracked by an incomplete recovery of the shape compared to baseline deformations or forces (Català-Castro et al., 2021). In addition, strain stiffening or stress softening can become

visible upon an increase or decrease in the force during repetitive indentations, respectively (Andreu et al., 2021; Mehidi et al., 2021). Likewise, active processes violate the fluctuation–dissipation theorem, and material properties cannot be derived from passive microrheology experiments alone (Turlier et al., 2016). Thus, the age and metabolic state of a tissue culture needs to be carefully controlled to prevent artifacts and ensure reproducibility of measurements. In summary, more advanced models to relate force and deformation in complex media and at interfaces, for example, at the cell surface or the nuclear envelope, are needed, which combine genetics (Das et al., 2021), pharmacological perturbations (Venturini et al., 2020) and clever experimental interrogations (Mehidi et al., 2021) to decipher the mechanical footprint of living materials.

Conclusions

Optical tweezers can be used to create 3D viscoelasticity maps inside living cells and complex mechanical environments. The small size of a laser focus and the ability for subdiffraction sensing and manipulation with nanometer precision and subpiconewton force resolution make optical tweezers a perfect tool for the study the mechanics of cells. Direct momentum-based force measurements enable quantitative measurements inside cells and allow force measurements beyond the linear Hookean regime. The temporal resolution and fast response time of optical tweezers with high refractive index nanospheres allow the mapping of the microsecond dynamics of walking molecular motors (Sudhakar et al., 2021). Furthermore, the non-invasive operation with infrared light enables deep cell penetration, can resolve single-molecule forces in living cells, and does not spectrally overlap with common genetically encoded fluorescent biosensors. Thus, multimodal interrogation of force and function in living specimens are possible. In the future, the use of novel nano- and micro-particles as trapping probes, combined with adaptive optics, will allow researchers to measure even deeper and faster with higher forces to enter an as-yet unexplored territory of cell biology and tissue biophysics.

Acknowledgements

We would like to thank the members of the NMSB lab for discussion and sharing unpublished material.

Competing interests

The authors declare no competing or financial interests.

Funding

E.S. acknowledges the Deutsche Forschungsgemeinschaft [DFG; CRC 1101, Project A04 and the Research Training Group (RTG) MOMbrane-GRK 2364] and the University of Tübingen. M.K. acknowledges support from the European Research Council (ERC; 715243), Human Frontiers Science Program (HFSP; CDA00023/2018), Spanish Ministry (PGC2018-097882-A-I00, EQC2018-005048-P), Fundación Carmen y Severo Ochoa program for Centres of Excellence in R&D (CEX2019-000910-S; RYC-2016-21062).

References

Abe, Y., Meguriya, K., Matsuzaki, T., Sugiyama, T., Yoshikawa, H. Y., Morita, M. T. and Toyota, M. (2020). Micromanipulation of amyloplasts with optical tweezers in arabidopsis stems. *Plant Biotechnol.* **37**, 405-415. doi:10.5511/plantbiotechnology.20.1201a

Abeytunge, S., Gianoli, F., Hudspeth, A. J. and Kozlov, A. S. (2021). Rapid mechanical stimulation of inner-ear hair cells by photonic pressure. *Elife* **10**, e65930. doi:10.7554/eLife.65930

Ahmed, W. W., Fodor, É., Almonacid, M., Bussonnier, M., Verlhac, M. H., Gov, N., Visco, P., van Wijland, F. and Betz, T. (2018). Active mechanics reveal molecular-scale force kinetics in living oocytes. *Biophys. J.* **114**, 1667-1679. doi:10.1016/j.bpj.2018.02.009

Alibert, C., Pereira, D., Lardier, N., Etienne-Manneville, S., Goud, B., Asnacios, A. and Manneville, J. B. (2021). Multiscale rheology of glioma cells. *Biomaterials* **275**, 120903. doi:10.1016/j.biomaterials.2021.120903

Alshareedah, I., Moosa, M. M., Pham, M., Potoyan, D. A. and Banerjee, P. R. (2021). Programmable viscoelasticity in protein-RNA condensates with disordered sticker-spacer polypeptides. *Nat. Commun.* **12**, 6620. doi:10.1038/s41467-021-26733-7

Andersson, M. X., Goksör, M. and Sandelius, A. S. (2007). Optical manipulation reveals strong attracting forces at membrane contact sites between endoplasmic reticulum and chloroplasts. *J. Biol. Chem.* **282**, 1170-1174. doi:10.1074/jbc.M608124200

Andres-arroyo, A., Wang, F., Toe, W. J. and Reece, P. (2015). Intrinsic heating in optically trapped Au nanoparticles measured by dark-field spectroscopy. *Biomed. Opt. Express* **6**, 2256-2262. doi:10.1364/BOE.6.003646

Andreu, I., Falcones, B., Hurst, S., Chahare, N., Quiroga, X., Le Roux, A. L., Kechagia, Z., Beedle, A. E. M., Elosegui-Artola, A., Trepat, X. et al. (2021). The force loading rate drives cell mechanosensing through both reinforcement and cytoskeletal softening. *Nat. Commun.* **12**, 4229. doi:10.1038/s41467-021-24383-3

Ashkin, A. and Dziedzic, J. M. (1987). Optical trapping and manipulation of viruses and bacteria. *Science (80-.)* **235**, 1517-1520. doi:10.1126/science.3547653

Ashkin, A., Dziedzic, J. M., Bjorkholm, J. E. and Chu, S. (1986). Observation of a single-beam gradient force optical trap for dielectric particles. *Opt. Lett.* **11**, 196-198. doi:10.1364/OL.11.000288

Ashkin, A., Dziedzic, J. M. and Yamane, T. (1987). Optical trapping and manipulation of single cells using infrared laser beams. *Nature* **330**, 769-771. doi:10.1038/330769a0

Ayala, Y. A., Pontes, B., Ether, D. S., Pires, L. B., Araujo, G. R., Frases, S., Romão, L. F., Farina, M., Moura-Neto, V., Viana, N. B. et al. (2016). Rheological properties of cells measured by optical tweezers. *BMC Biophys.* **9**, 5. doi:10.1186/s13628-016-0031-4

Bambardekar, K., Clément, R., Blanc, O., Chardès, C. and Lenne, P. F. (2015). Direct laser manipulation reveals the mechanics of cell contacts in vivo. *Proc. Natl. Acad. Sci. USA* **112**, 1416-1421. doi:10.1073/pnas.1418732112

Barak, P., Rai, A., Rai, P. and Mallik, R. (2013). Quantitative optical trapping on single organelles in cell extract. *Nat. Methods* **10**, 68-70. doi:10.1038/nmeth.2287

Berg-Sørensen, K. and Flyvbjerg, H. (2004). Power spectrum analysis for optical tweezers. *Rev. Sci. Instrum.* **75**, 594-612. doi:10.1063/1.1645654

Berghoff, K., Gross, W., Eisentraut, M. and Kress, H. (2021). Using blinking optical tweezers to study cell rheology during initial cell-particle contact. *Biophys. J.* **120**, 3527-3537. doi:10.1016/j.bpj.2021.04.034

Blehm, B. H., Schroer, T. A., Trybus, K. M., Chemla, Y. R. and Selvin, P. R. (2013). In vivo optical trapping indicates kinesin's stall force is reduced by dynein during intracellular transport. *Proc. Natl. Acad. Sci. USA* **110**, 9613. doi:10.1073/pnas.1219961110

Blehm, B. H., Devine, A., Staunton, J. R. and Tanner, K. (2016). In vivo tissue has non-linear rheological behavior distinct from 3D biomimetic hydrogels, as determined by AMOTIV microscopy. *Biomaterials* **83**, 66-78. doi:10.1016/j.biomaterials.2015.12.019

Bonfanti, A., Fouchard, J., Khalilgharibi, N., Charras, G. and Kabla, A. (2019). A unified rheological model for cells and cellularised materials. *R. Soc. Open Sci.* **7**, 190920. doi:10.1098/rsos.190920

Bonfanti, A., Kaplan, J. L., Charras, G. and Kabla, A. (2020). Fractional viscoelastic models for power-law materials. *Soft Mat.* **16**, 6002-6020. doi:10.1039/D0SM00354A

Boothe, T., Hilbert, L., Heide, M., Berninger, L., Huttner, W. B., Zaburdaev, V., Vastenhouw, N. L., Myers, E. W., Drechsel, D. N. and Rink, J. C. (2017). A tunable refractive index matching medium for live imaging cells, tissues and model organisms. *Elife* **6**, e27240. doi:10.7554/eLife.27240

Bormuth, V., Jannasch, A., Ander, M., van Kats, C. M., van Blaaderen, A., Howard, J. and Schaffer, E. (2008). Optical trapping of coated microspheres. *Opt. Express* **16**, 13831-13844. doi:10.1364/OE.16.013831

Bormuth, V., Varga, V., Howard, J. and Schäffer, E. (2009). Protein friction limits diffusive and directed movements of kinesin motors on microtubules. *Science* **325**, 870-873. doi:10.1126/science.1174923

Brochard-Wyart, F., Borghi, N., Cuvelier, D. and Nassoy, P. (2006). Hydrodynamic narrowing of tubes extruded from cells. *Proc. Natl. Acad. Sci. USA* **103**, 7660-7663. doi:10.1073/pnas.0602012103

Bugiel, M., Jannasch, A. and Schaffer, E. (2017). Implementation and tuning of an optical tweezers force-clamp feedback system. In *Optical Tweezers: Methods and Protocols, Methods in Molecular Biology* (ed. Arne Gennerich), pp. 109-136. Springer.

Bui, A. A. M., Kashchuk, A. V., Balanant, M. A., Nieminen, T. A., Rubinsztein-Dunlop, H. and Stilgoe, A. B. (2018). Calibration of force detection for arbitrarily shaped particles in optical tweezers. *Sci. Rep.* **8**, 10798. doi:10.1038/s41598-018-28876-y

Bustamante, C. J., Chemla, Y. R., Liu, S. and Wang, M. D. (2021). Optical tweezers in single-molecule biophysics. *Nat. Rev. Methods Prim.* **1**, 25. doi:10.1038/s43586-020-00001-2

Callegari, A., Mijalkov, M., Burak Gököz, A. and Volpe, G. (2019). Computational toolbox for optical tweezers in the geometrical optics regime. In *Biophotonics Congress: Optics in the Life Sciences Congress 2019 (BODA,BRAIN,NTM,OMA,*

OMP), OSA Technical Digest (Optica Publishing Group, 2019), paper AT3E.6. doi:10.1364/OMA.2019.AT3E.6
Català-Castro, F. and Martín-Badosa, E. (2021). Positioning accuracy in holographic optical traps. *Micromachines* **12**, 559. doi:10.3390/mi12050559
Català-Castro, F., Venturini, V., Ortiz-Vásquez, S., Ruprecht, V. and Krieg, M. (2021). Direct force measurements of subcellular mechanics in confinement using optical tweezers. *J. Vis. Exp.* **174**, e62865. doi:10.3791/62865
Català, F., Marsà, F., Montes-Usategui, M., Farré, A. and Martín-Badosa, E. (2017a). Extending calibration-free force measurements to optically-trapped rod-shaped samples. *Sci. Rep.* **7**, 42960. doi:10.1038/s41598-016-0028-x
Català, F., Marsà, F., Montes-Usategui, M., Farré, A. and Martín-Badosa, E. (2017b). Influence of experimental parameters on the laser heating of an optical trap. *Sci. Rep.* **7**, 16052. doi:10.1038/s41598-017-15904-6
Chardès, C., Clement, R., Blanc, O. and Lenne, P. F. (2018). Probing cell mechanics with bead-free optical tweezers in the drosophila embryo. *J. Vis. Exp.* **141**, e57900. doi:10.3791/57900
Charras, G. T., Yarrow, J. C., Horton, M. A., Mahadevan, L. and Mitchison, T. J. (2005). Non-equilibration of hydrostatic pressure in blebbing cells. *Nature* **435**, 365-369. doi:10.1038/nature03550
Chen, D. T. N., Wen, Q., Janmey, P. A., Crocker, J. C. and Yodh, A. G. (2010). Rheology of soft materials. *Annu. Rev. Condens. Matter Phys.* **1**, 301-322. doi:10.1146/annurev-conmatphys-070909-104120
Chen, B., Brinkmann, K., Chen, Z., Pak, C. W., Liao, Y., Shi, S., Henry, L., Grishin, N. V., Bogdan, S. and Rosen, M. K. (2014). The WAVE regulatory complex links diverse receptors to the actin cytoskeleton. *Cell* **156**, 195-207. doi:10.1016/j.cell.2013.11.048
Cohen, A. E. and Shi, Z. (2019). Do cell membranes flow like honey or jiggle like jello? *BioEssays* **42**, e1900142. doi:10.1002/bies.201900142
Cordova, J. C., Reinemann, D. N., Laky, D. J., Hesse, W. R., Tushak, S. K., Weltman, Z. L., Best, K. B., Bardhan, R. and Lang, M. J. (2018). Bioconjugated core–shell microparticles for high-force optical trapping. *Part. Part. Syst. Charact.* **35**, 1700448. doi:10.1002/ppsc.201700448
Dai, J. and Sheetz, M. P. (1995a). Axon membrane flows from the growth cone to the cell body. *Cell* **83**, 693-701. doi:10.1016/0092-8674(95)90182-5
Dai, J. and Sheetz, M. P. (1995b). Mechanical properties of neuronal growth cone membranes studied by tether formation with laser optical tweezers. *Biophys. J.* **68**, 988-996. doi:10.1016/S0006-3495(95)80274-2
Dai, J., Sheetz, M. P., Wan, X. and Morris, C. E. (1998). Membrane tension in swelling and shrinking molluscan neurons. *J. Neurosci.* **18**, 6681-6692. doi:10.1523/JNEUROSCI.18-17-06681.1998
Das, R., Lin, L. C., Català-Castro, F., Malaiwong, N., Sanfeliu-Cerdán, N., Porta-De-la-Riva, M., Pidde, A. and Krieg, M. (2021). An asymmetric mechanical code ciphers curvature-dependent proprioceptor activity. *Sci. Adv.* **7**, eabg4617. doi:10.1126/sciadv.abg4617
Datar, A., Bornschlögl, T., Bassereau, P., Prost, J. and Pullarkat, P. A. (2015). Dynamics of membrane tethers reveal novel aspects of cytoskeleton-membrane interactions in axons. *Biophys. J.* **108**, 489-497. doi:10.1016/j.bpj.2014.11.3480
Dufresne, E. R., Spalding, G. C., Dearing, M. T., Sheets, S. A. and Grier, D. G. (2001). Computer-generated holographic optical tweezer arrays. *Rev. Sci. Instrum.* **72**, 1810-1816. doi:10.1063/1.1344176
Dumont, S. and Prakash, M. (2014). Emergent mechanics of biological structures. *Mol. Biol. Cell* **25**, 3461-3465. doi:10.1091/mbc.e14-03-0784
Dutra, R. S., Viana, N. B., Maia Neto, P. A. and Nussenzveig, H. M. (2014). Absolute calibration of forces in optical tweezers. *Phys. Rev. A At. Mol. Opt. Phys.* **90**, 013825. doi:10.1103/PhysRevA.90.013825
Dzementsei, A., Barooji, Y. F., Ober, E. A. and Oddershede, L. B. (2022). Foregut organ progenitors and their niche display distinct viscoelastic properties in vivo during early morphogenesis stages. *Commun. Biol.* **5**, 402. doi:10.1038/s42003-022-03349-1
Efremov, Y. M., Velay-Lizancos, M., Weaver, C. J., Athamneh, A. I., Zavattieri, P. D., Suter, D. M. and Raman, A. (2019). Anisotropy vs isotropy in living cell indentation with AFM. *Sci. Rep.* **9**, 5757. doi:10.1038/s41598-019-42077-1
Ekpenyong, A. E., Whyte, G., Chalut, K., Pagliara, S., Lautenschläger, F., Fiddler, C., Paschke, S., Keyser, U. F., Chilvers, E. R. and Guck, J. (2012). Viscoelastic properties of differentiating blood cells are fate- and function-dependent. *PLoS One* **7**, e45237. doi:10.1371/journal.pone.0045237
Evans, E. A. and Calderwood, D. A. (2007). Forces and bond dynamics in cell adhesion. *Science* **316**, 1148-1153. doi:10.1126/science.1137592
Falleroni, F., Torre, V. and Cojoc, D. (2018). Cell mechanotransduction with piconewton forces applied by optical tweezers. *Front. Cell. Neurosci.* **12**, 130. doi:10.3389/fncel.2018.00130
Farré, A. and Montes-Usategui, M. (2010). A force detection technique for single-beam optical traps based on direct measurement of light momentum changes. *Opt. Express* **18**, 11955. doi:10.1364/OE.18.011955
Farré, A., Marsà, F. and Montes-Usategui, M. (2012). Optimized back-focal-plane interferometry directly measures forces of optically trapped particles. *Opt. Express* **20**, 12270. doi:10.1364/OE.20.012270
Farré, A., Marsà, F. and Montes-Usategui, M. (2017). Beyond the hookean spring model: Direct measurement of optical forces through light momentum changes. In *Optical Tweezers: Methods and Protocols, Methods in Molecular Biology* (ed. A. Gennerich), pp. 41-76. New York: Springer.
Favre-Bulle, I. A., Stilgoe, A. B., Rubinsztein-Dunlop, H. and Scott, E. K. (2017). Optical trapping of otoliths drives vestibular behaviours in larval zebrafish. *Nat. Commun.* **8**, 630. doi:10.1038/s41467-016-0009-6
Favre-Bulle, I. A., Vanwalleghem, G., Taylor, M. A., Rubinsztein-Dunlop, H. and Scott, E. K. (2018). Cellular-resolution imaging of vestibular processing across the larval Zebrafish brain. *Curr. Biol.* **28**, 3711-3722.e3. doi:10.1016/j.cub.2018.09.060
Favre-Bulle, I. A., Stilgoe, A. B., Scott, E. K. and Rubinsztein-Dunlop, H. (2019). Optical trapping in vivo: theory, practice, and applications. *Nanophotonics* **8**, 1023-1040. doi:10.1515/nanoph-2019-0055
Feng, Q. and Kornmann, B. (2018). Mechanical forces on cellular organelles. *J. Cell Sci.* **131**, jcs218479. doi:10.1242/jcs.218479
Ferro, V., Sonnberger, A., Abdosamadi, M. K., McDonald, C., Schäffer, E. and McGloin, D. (2016). Improved antireflection coated microspheres for biological applications of optical tweezers. *Opt. Trapp. Opt. Micromanipulation* **9922**, 99222T. doi:10.1117/12.2239025
Ferro, V., Chuai, M., McGloin, D. and Weijer, C. J. (2020). Measurement of junctional tension in epithelial cells at the onset of primitive streak formation in the chick embryo via non-destructive optical manipulation. *Development* **147**, dev175109. doi:10.1242/dev.175109
Florin, E. L., Pralle, A., Heinrich Hörber, J. K. and Stelzer, E. H. K. (1997). Photonic force microscope based on optical tweezers and two-photon excitation for biological applications. *J. Struct. Biol.* **119**, 202-211. doi:10.1006/jsbi.1997.3880
Gao, H., Metz, J., Teanby, N. A., Ward, A. D., Botchway, S. W., Coles, B., Pollard, M. R. and Sparkes, I. (2016). In vivo quantification of peroxisome tethering to chloroplasts in tobacco epidermal cells using optical tweezers1[OPEN]. *Plant Physiol.* **170**, 263-272. doi:10.1104/pp.15.01529
Gárate, F., Betz, T., Pertusa, M. and Bernal, R. (2015). Time-resolved neurite mechanics by thermal fluctuation assessments. *Phys. Biol.* **12**, 066020. doi:10.1088/1478-3975/12/6/066020
Ghosh, A., Kota, D. and Zhou, H.-X. (2021). Shear relaxation governs fusion dynamics of biomolecular condensates. *Nat. Commun.* **12**, 5995. doi:10.1038/s41467-020-20314-w
Gieseler, J., Gomez-Solano, J. R., Magazzù, A., Pérez Castillo, I., Pérez García, L., Gironella-Torrent, M., Viader-Godoy, X., Ritort, F., Pesce, G., Arzola, A. V. et al. (2021). Optical tweezers — from calibration to applications: a tutorial. *Adv. Opt. Photonics* **13**, 74. doi:10.1364/AOP.394888
Gittes, F. and Schmidt, C. F. (1998). Interference model for back-focal-plane displacement detection in optical tweezers. *Opt. Lett.* **23**, 7. doi:10.1364/OL.23.000007
Gomis Perez, C., Dudzinski, N. R., Rouches, M., Machta, B., Zenisek, D. and Karatekin, E. (2022). Rapid propagation of membrane tension at a presynaptic terminal. *Sci. Adv.* **4411**, eabl4411. doi:10.1126/sciadv.abl4411
Guck, J., Schinkinger, S., Lincoln, B., Wottawah, F., Ebert, S., Romeyke, M., Lenz, D., Erickson, H. M., Ananthakrishnan, R., Mitchell, D. et al. (2005). Optical deformability as an inherent cell marker for testing malignant transformation and metastatic competence. *Biophys. J.* **88**, 3689-3698. doi:10.1529/biophysj.104.045476
Guet, D., Mandal, K., Pinot, M., Hoffmann, J., Abidine, Y., Sigaut, W., Bardin, S., Schauer, K. and Goud, B. (2014). Article mechanical role of actin dynamics in the rheology of the golgi complex and in golgi-associated trafficking events. *Curr. Biol.* **24**, 1700-1711. doi:10.1016/j.cub.2014.06.048
Guilford, W. H., Tournas, J. A., Dascalu, D. and Watson, D. S. (2004). Creating multiple time-shared laser traps with simultaneous displacement detection using digital signal processing hardware. *Anal. Biochem.* **326**, 153-166. doi:10.1016/j.ab.2003.11.025
Guo, M., Ehrlicher, A. J., Mahammad, S., Fabich, H., Jensen, M. H., Moore, J. R., Fredberg, J. J., Goldman, R. D. and Weitz, D. A. (2013). The role of vimentin intermediate filaments in cortical and cytoplasmic mechanics. *Biophysj* **105**, 1562-1568. doi:10.1016/j.bpj.2013.08.037
Guo, M., Ehrlicher, A. J., Jensen, M. H., Renz, M., Moore, J. R., Goldman, R. D., Lippincott-Schwartz, J., Mackintosh, F. C. and Weitz, D. A. (2014). Probing the stochastic, motor-driven properties of the cytoplasm using force spectrum microscopy. *Cell* **158**, 822-832. doi:10.1016/j.cell.2014.06.051
Guo, M., Pegoraro, A. F., Mao, A., Zhou, E. H., Arany, P. R. and Han, Y. (2017). Cell volume change through water efflux impacts cell stiffness and stem cell fate. *Proc. Natl. Acad. Sci. USA* **114**, 8618-8627.
Han, Y. L., Ronceray, P., Xu, G., Malandrino, A., Kamm, R. D., Lenz, M., Broedersz, C. P. and Guo, M. (2018). Cell contraction induces long-ranged stress stiffening in the extracellular matrix. *Proc. Natl. Acad. Sci. U. S. A.* **115**, 4075-4080. doi:10.1073/pnas.1722619115
Han, Y. L., Pegoraro, A. F., Li, H., Li, K., Yuan, Y., Xu, G., Gu, Z., Sun, J., Hao, Y., Gupta, S. K. et al. (2020). Cell swelling, softening and invasion in a three-dimensional breast cancer model. *Nat. Phys.* **16**, 101-108. doi:10.1038/s41567-019-0680-8

Harlepp, S., Thalmann, F., Follain, G. and Goetz, J. G. (2017). Hemodynamic forces can be accurately measured in vivo with optical tweezers. *Mol. Biol. Cell* **28**, 3252-3260. doi:10.1091/mbc.e17-06-0382

Hayakawa, K., Tatsumi, H. and Sokabe, M. (2008). Actin stress fibers transmit and focus force to activate mechanosensitive channels. *J. Cell Sci.* **121**, 496-503. doi:10.1242/jcs.022053

Hendricks, A. G., Holzbaur, E. L. F. and Goldman, Y. E. (2012). Force measurements on cargoes in living cells reveal collective dynamics of microtubule motors. *Proc. Natl. Acad. Sci. U. S. A.* **109**, 18447-18452. doi:10.1073/pnas.1215462109

Hochmuth, R. M., Shao, J. Y., Dai, J. and Sheetz, M. P. (1996). Deformation and flow of membrane into tethers extracted from neuronal growth cones. *Biophys. J.* **70**, 358-369. doi:10.1016/S0006-3495(96)79577-2

Hörner, F., Meissner, R., Polali, S., Pfeiffer, J., Betz, T., Denz, C. and Raz, E. (2017). Holographic optical tweezers-based in vivo manipulations in zebrafish embryos. *J. Biophotonics* **10**, 1492-1501. doi:10.1002/jbio.201600226

Houk, A. R., Jilkine, A., Mejean, C. O., Boltyanskiy, R., Dufresne, E. R., Angenent, S. B., Altschuler, S. J., Wu, L. F. and Weiner, O. D. (2012). Membrane tension maintains cell polarity by confining signals to the leading edge during neutrophil migration. *Cell* **148**, 175-188. doi:10.1016/j.cell.2011.10.050

Howard, J. (2001). *Mechanics of Motor Proteins and the Cytoskeleton*. Sinauer Associates, Inc.

Hu, J., Jafari, S., Han, Y., Grodzinsky, A. J., Cai, S. and Guo, M. (2017). Size- and speed-dependent mechanical behavior in living mammalian cytoplasm. *Proc. Natl. Acad. Sci. U. S. A.* **114**, 9529-9534. doi:10.1073/pnas.1702488114

Hu, J., Li, Y., Hao, Y., Zheng, T., Gupta, S. K., Alberto, G. and Wu, H. (2019). High stretchability, strength, and toughness of living cells enabled by hyperelastic vimentin intermediate filaments. *Proc. Natl. Acad. Sci. USA* **116**, 17175-17180. doi:10.1073/pnas.1903890116

Huhle, A., Klaue, D., Brutzer, H., Daldrop, P., Joo, S., Otto, O., Keyser, U. F. and Seidel, R. (2015). Camera-based three-dimensional real-time particle tracking at kHz rates and Ångström accuracy. *Nat. Commun.* **6**, 5885. doi:10.1038/ncomms6885

Huisstede, J. H. G., van der Werf, K. O., Bennink, M. L. and Subramaniam, V. (2005). Force detection in optical tweezers using backscattered light. *Opt. Express* **13**, 1113. doi:10.1364/OPEX.13.001113

Hurst, S., Vos, B. E., Brandt, M. and Betz, T. (2021). Intracellular softening and increased viscoelastic fluidity during division. *Nat. Phys.* **17**, 1270-1276. doi:10.1038/s41567-021-01368-z

Jannasch, A., Mahamdeh, M. and Schäffer, E. (2011). Inertial effects of a small brownian particle cause a colored power spectral density of thermal noise. *Phys. Rev. Lett.* **107**, 228301. doi:10.1103/PhysRevLett.107.228301

Jannasch, A., Demirörs, A. F., Van Oostrum, P. D. J., Van Blaaderen, A. and Schäffer, E. (2012). Nanonewton optical force trap employing anti-reflection coated, high-refractive-index titania microspheres. *Nat. Photonics* **6**, 469-476. doi:10.1038/nphoton.2012.140

Jawerth, L. M., Ijavi, M., Ruer, M., Saha, S., Jahnel, M., Hyman, A. A., Jülicher, F. and Fischer-Friedrich, E. (2018). Salt-dependent rheology and surface tension of protein condensates using optical traps. *Phys. Rev. Lett.* **121**, 258101. doi:10.1103/PhysRevLett.121.258101

Jawerth, L., Fischer-Friedrich, E., Saha, S., Wang, J., Franzmann, T., Zhang, X., Sachweh, J., Ruer, M., Ijavi, M., Saha, S. et al. (2020). Protein condensates as aging Maxwell fluids. *Science* **370**, 1317-1323. doi:10.1126/science.aaw4951

Johansen, P. L., Fenaroli, F., Evensen, L., Griffiths, G. and Koster, G. (2016). Optical micromanipulation of nanoparticles and cells inside living zebrafish. *Nat. Commun.* **7**, 10974. doi:10.1038/ncomms10974

Kariuki, S. N., Marin-Menendez, A., Introini, V., Ravenhill, B. J., Lin, Y. C., Macharia, A., Makale, J., Tendwa, M., Nyamu, W., Kotar, J. et al. (2020). Red blood cell tension protects against severe malaria in the Dantu blood group. *Nature* **585**, 579-583. doi:10.1038/s41586-020-2726-6

Ketelaar, T., Faivre-Moskalenko, C., Esseling, J. J., De Ruijter, N. C. A., Grierson, C. S., Dogterom, M. and Emons, A. M. C. (2002). Positioning of nuclei in Arabidopsis root hairs: an actin-regulated process of tip growth. *Plant Cell* **14**, 2941-2955. doi:10.1105/tpc.005892

Khalilgharibi, N., Fouchard, J., Asadipour, N., Barrientos, R., Duda, M., Bonfanti, A., Yonis, A., Harris, A., Mosaffa, P., Fujita, Y. et al. (2019). Stress relaxation in epithelial monolayers is controlled by the actomyosin cortex. *Nat. Phys.* **15**, 839-847. doi:10.1038/s41567-019-0516-6

Khan, M., Regan, K. and Robertson-Anderson, R. M. (2019). Optical tweezers microrheology maps the dynamics of strain-induced local inhomogeneities in entangled polymers. *Phys. Rev. Lett.* **123**, 38001. doi:10.1103/PhysRevLett.123.038001

Kim, T., Joo, C., Seong, J., Vafabakhsh, R., Botvinick, E. L., Berns, M. W., Palmer, A. E., Wang, N., Ha, T. and Jakobsson, E. (2015). Distinct mechanisms regulating mechanical force-induced Ca 2+signals at the plasma membrane and the ER in human MSCs. *Elife* **4**, e04876. doi:10.7554/eLife.04876

Koster, G., Cacciuto, A., Derényi, I., Frenkel, D. and Dogterom, M. (2005). Force barriers for membrane tube formation. *Phys. Rev. Lett.* **94**, 68101. doi:10.1103/PhysRevLett.94.068101

Krieg, M., Fläschner, G., Alsteens, D., Gaub, B. M., Roos, W. H., Wuite, G. J. L., Gaub, H. E., Gerber, C., Dufrêne, Y. F. and Müller, D. J. (2019). Atomic force microscopy-based mechanobiology. *Nat. Rev. Phys.* **1**, 41-57. doi:10.1038/s42254-018-0001-7

Krieg, M., Pidde, A. and Das, R. (2022). Mechanosensitive Body-Brain Interactions in C. elegans. *Curr. Opin Neurobiol.* **75**, 102574. doi:10.1016/j.conb.2022.102574

Lang, M. J., Asbury, C. L., Shaevitz, J. W. and Block, S. M. (2002). An automated two-dimensional optical force clamp for single molecule studies. *Biophys. J.* **83**, 491-501. doi:10.1016/S0006-3495(02)75185-0

Latorre, E., Kale, S., Casares, L., Gómez-González, M., Uroz, M., Valon, L., Nair, R. V., Garreta, E., Montserrat, N., del Campo, A. et al. (2018). Active superelasticity in three-dimensional epithelia of controlled shape. *Nature* **563**, 203-208. doi:10.1038/s41586-018-0671-4

Lee, H., Ferrer, J. M., Lang, M. J. and Kamm, R. D. (2010). Molecular origin of strain softening in cross-linked F-actin networks. *Phys. Rev. E Stat. Nonlinear, Soft Matter Phys.* **82**, 20-23.

Leijnse, N., Oddershede, L. B. and Bendix, P. M. (2014). Helical buckling of actin inside filopodia generates traction. *Proc. Natl. Acad. Sci. USA* **112**, 136-141. doi:10.1073/pnas.1411761112

Leitz, G., Fällman, E., Tuck, S. and Axner, O. (2002). Stress response in Caenorhabditis elegans caused by optical tweezers: Wavelength, power, and time dependence. *Biophys. J.* **82**, 2224-2231. doi:10.1016/S0006-3495(02)75568-9

Leitz, G., Kang, B. H. and Schoenwaelder, M. E. A. (2009). Statolith sedimentation kinetics and force transduction to the cortical endoplasmic reticulum in gravity-sensing Arabidopsis columella cells. *Plant Cell* **21**, 843-860. doi:10.1105/tpc.108.065052

Lenton, I. C. D., Stilgoe, A. B., Rubinsztein-Dunlop, H. and Nieminen, T. A. (2017). Visual guide to optical tweezers. *Eur. J. Phys.* **38**, 177-181.

Lieber, A. D., Schweitzer, Y., Kozlov, M. M. and Keren, K. (2015). Front-to-rear membrane tension gradient in rapidly moving cells. *Biophys. J.* **108**, 1599-1603. doi:10.1016/j.bpj.2015.02.007

López-Quesada, C., Fontaine, A.-S., Farré, A., Joseph, M., Selva, J., Egea, G., Ludevid, M. D., Martín-Badosa, E. and Montes-Usategui, M. (2014). Artificially-induced organelles are optimal targets for optical trapping experiments in living cells. *Biomed. Opt. Express* **5**, 1993. doi:10.1364/BOE.5.001993

Ma, R. and Berro, J. (2021). Endocytosis against high turgor pressure is made easier by partial coating and freely rotating base. *Biophys. J.* **120**, 1625-1640. doi:10.1016/j.bpj.2021.02.033

Mahamdeh, M. and Schäffer, E. (2009). Optical tweezers with millikelvin precision of temperature-controlled objectives and base-pair resolution. *Opt. Express* **17**, 17190. doi:10.1364/OE.17.017190

Mahamdeh, M., Pérez Campos, C. and Schäffer, E. (2011). Under-filling trapping objectives optimizes the use of the available laser power in optical tweezers. *Opt. Express* **19**, 11759. doi:10.1364/OE.19.011759

Majumdar, S., Foucard, L. C., Levine, A. J. and Gardel, M. L. (2018). Mechanical hysteresis in actin networks. *Soft Mat.* **14**, 2052-2058. doi:10.1039/C7SM01948C

Mandal, K., Asnacios, A., Goud, B. and Manneville, J. (2016). Mapping intracellular mechanics on micropatterned substrates. *Proc. Natl. Acad. Sci. USA* **113**, 7159-7168. doi:10.1073/pnas.1605112113

Mandal, K., Pogoda, K., Nandi, S., Mathieu, S., Kasri, A., Klein, E., Goud, B., Janmey, P. A. and Manneville, J. (2019). Role of a kinesin motor in cancer cell mechanics. *Nano Lett.* **19**, 7691-7702. doi:10.1021/acs.nanolett.9b02592

Mason, T. G. and Weitz, D. A. (1995). Optical measurements of frequency-dependent linear viscoelastic moduli of complex fluids. *Phys. Rev. Lett.* **74**, 1250-1253. doi:10.1103/PhysRevLett.74.1250

Masters, T. A., Pontes, B., Viasnoff, V., Li, Y. and Gauthier, N. C. (2013). Plasma membrane tension orchestrates membrane trafficking, cytoskeletal remodeling, and biochemical signaling during phagocytosis. *Proc. Natl. Acad. Sci. U. S. A.* **110**, 11875-11880. doi:10.1073/pnas.1301766110

Mehidi, A., Kage, F., Karatas, Z., Cercy, M., Schaks, M., Polesskaya, A., Sainlos, M., Gautreau, A. M., Rossier, O., Rottner, K. et al. (2021). Forces generated by lamellipodial actin filament elongation regulate the WAVE complex during cell migration. *Nat. Cell Biol.* **23**, 1148-1162. doi:10.1038/s41556-021-00786-8

Mejean, C. O., Schaefer, A. W., Millman, E. A., Forscher, P. and Dufresne, E. R. (2009). Multiplexed force measurements on live cells with holographic optical tweezers. *Opt. Express* **17**, 6209. doi:10.1364/OE.17.006209

Meloty-Kapella, L., Shergill, B., Kuon, J., Botvinick, E. and Weinmaster, G. (2012). Notch ligand endocytosis generates mechanical pulling force dependent on dynamin, Epsins, and actin. *Dev. Cell* **22**, 1299-1312. doi:10.1016/j.devcel.2012.04.005

Merkel, R., Nassoy, P., Leung, A., Ritchie, K. and Evans, E. (1999). Energy landscapes of receptor-ligand bonds explored with dynamic force spectroscopy. *Nature* **397**, 50-53. doi:10.1038/16219

Mizuno, D., Head, D. A., MacKintosh, F. C. and Schmidt, C. F. (2008). Active and passive microrheology in equilibrium and nonequilibrium systems. *Macromolecules* **41**, 7194-7202. doi:10.1021/ma801218z

Nader, G. P. F., Williart, A. and Piel, M. (2021). Nuclear deformations, from signaling to perturbation and damage. *Curr. Opin. Cell Biol.* **72**, 137-145. doi:10.1016/j.ceb.2021.07.008

Neuman, K. C. and Block, S. M. (2004). Optical trapping. *Rev. Sci. Instrum.* **75**, 2787-2809. doi:10.1063/1.1785844
Neupane, K., Foster, D. A. N., Dee, D. R., Yu, H., Wang, F. and Woodside, M. T. (2016). Direct observation of transition paths during the folding of proteins and nucleic acids. *Science (80-.)* **352**, 239-243. doi:10.1126/science.aad0637
Nieminen, T. A., Loke, V. L. Y., Stilgoe, A. B., Knöner, G., Brańczyk, A. M., Heckenberg, N. R. and Rubinsztein-Dunlop, H. (2007). Optical tweezers computational toolbox. *J. Opt. A Pure Appl. Opt.* **9**, S196-S203. doi:10.1088/1464-4258/9/8/S12
Niethammer, P. (2021). Components and mechanisms of nuclear mechanotransduction. *Annu. Rev. Cell Dev. Biol.* **37**, 233-256. doi:10.1146/annurev-cellbio-120319-030049
Novikova, E. A. and Storm, C. (2013). Contractile fibers and catch-bond clusters: a biological force sensor? *Biophys. J.* **105**, 1336-1345. doi:10.1016/j.bpj.2013.07.039
Nussenzveig, H. M. (2017). Cell membrane biophysics with optical tweezers. *Eur. Biophys. J.* **47**, 499-514. doi:10.1007/s00249-017-1268-9
Osterrieder, A., Sparkes, I. A., Botchway, S. W., Ward, A., Ketelaar, T., de Ruijter, N. , and Hawes, C. (2017). Stacks off tracks: a role for the golgin AtCASP in plant endoplasmic reticulum-Golgi apparatus tethering. *J. Exp. Bot.* **68**, 3339-3350. doi:10.1093/jxb/erx167
Peterman, E. J., Gittes, F. and Schmidt, C. F. (2003). Laser-induced heating in optical traps. *Biophys. J.* **84**, 1308-1316. doi:10.1016/S0006-3495(03)74946-7
Pompeu, P., Lourenço, P. S., Ether, D. S., Soares, J., Farias, J., Maciel, G., Viana, N. B., Nussenzveig, H. M. and Pontes, B. (2021). Protocol to measure the membrane tension and bending modulus of cells using optical tweezers and scanning electron microscopy. *STAR Protoc.* **2**, 100283. doi:10.1016/j.xpro.2020.100283
Rai, A. K., Rai, A., Ramaiya, A. J., Jha, R. and Mallik, R. (2013). Molecular adaptations allow dynein to generate large collective forces inside cells. *Cell* **152**, 172-182. doi:10.1016/j.cell.2012.11.044
Rakshit, S., Zhang, Y., Manibog, K., Shafraz, O. and Sivasankar, S. (2012). Ideal, catch, and slip bonds in cadherin adhesion. *Proc. Natl. Acad. Sci. USA* **109**, 18815-18820. doi:10.1073/pnas.1208349109
Raucher, D. and Sheetz, M. P. (1999). Characteristics of a membrane reservoir buffering membrane tension. *Biophys. J.* **77**, 1992-2002. doi:10.1016/S0006-3495(99)77040-2
Raucher, D. and Sheetz, M. P. (2000). Cell spreading and lamellipodial extension rate is regulated by membrane tension. *J. Cell Biol.* **148**, 127-136. doi:10.1083/jcb.148.1.127
Reuten, R., Zendehroud, S., Nicolau, M., Fleischhauer, L., Laitala, A., Kiderlen, S., Nikodemus, D., Wullkopf, L., Nielsen, S. R., McNeilly, S. et al. (2021). Basement membrane stiffness determines metastases formation. *Nat. Mater.* **20**, 892-903. doi:10.1038/s41563-020-00894-0
Riesenberg, C., Iriarte-Valdez, C. A., Becker, A., Dienerowitz, M., Heisterkamp, A., Ngezahayo, A. and Torres-Mapa, M. L. (2020). Probing ligand-receptor interaction in living cells using force measurements with optical tweezers. *Front. Bioeng. Biotechnol.* **8**, 598459. doi:10.3389/fbioe.2020.598459
Roca-Cusachs, P., Conte, V. and Trepat, X. (2017). Quantifying forces in cell biology. *Nat. Cell Biol.* **19**, 742-751. doi:10.1038/ncb3564
Sanfeliu-Cerdán, N., Mateos, B., Garcia-Cabau, C., Català-Castro, F., Ribera, M., Ruider, I., Porta-de-la-Riva, M., Wieser, S., Salvatella, X. and Krieg, M. (2022). A rigidity phase transition of stomatin condensates governs a switch from transport to mechanotransduction. *bioRxiv* 2022.07.08.499356. doi:10.1101/2022.07.08.499356
Schäffer, E., Nørrelykke, S. F. and Howard, J. (2007). Surface forces and drag coefficients of microspheres near a plane surface measured with optical tweezers. *Langmuir* **23**, 3654-3665. doi:10.1021/la0622368
Schürmann, M., Scholze, J., Müller, P., Guck, J. and Chan, C. J. (2016). Cell nuclei have lower refractive index and mass density than cytoplasm. *J. Biophotonics* **9**, 1068-1076. doi:10.1002/jbio.201500273
Shan, X., Wang, F., Wang, D., Wen, S., Chen, C., Di, X., Nie, P., Liao, J., Liu, Y., Ding, L. et al. (2021). Optical tweezers beyond refractive index mismatch using highly doped upconversion nanoparticles. *Nat. Nanotechnol.* **16**, 531-537. doi:10.1038/s41565-021-00852-0
Sharma, S., Subramani, S. and Popa, I. (2021). Does protein unfolding play a functional role in vivo?. *FEBS J.* **288**, 1742-1758. doi:10.1111/febs.15508
Sheetz, M. P. (2001). Cell control by membrane-cytoskeleton adhesion. *Nat. Rev. Mol. Cell Biol.* **2**, 392-396. doi:10.1038/35073095
Shen, Y., Ruggeri, F. S., Vigolo, D., Kamada, A., Qamar, S., Levin, A., Iserman, C., Alberti, S., George-Hyslop, P. S. and Knowles, T. P. J. (2020). Biomolecular condensates undergo a generic shear-mediated liquid-to-solid transition. *Nat. Nanotechnol.* **15**, 841-847. doi:10.1038/s41565-020-0731-4
Shi, Z., Graber, Z. T., Baumgart, T., Stone, H. A. and Cohen, A. E. (2018). Cell membranes resist flow. *Cell* **175**, 1769-1779.e13. doi:10.1016/j.cell.2018.09.054
Shubeita, G. T., Tran, S. L., Xu, J., Vershinin, M., Cermelli, S., Cotton, S. L., Welte, M. A. and Gross, S. P. (2008). Consequences of motor copy number on the intracellular transport of kinesin-1-driven lipid droplets. *Cell* **135**, 1098-1107. doi:10.1016/j.cell.2008.10.021
Sims, P. A. and Xie, X. S. (2009). Probing dynein and kinesin stepping with mechanical manipulation in a living cell. *Chemphyschem* **10**, 1511-1516. doi:10.1002/cphc.200900113
Singh, V. and Lamaze, C. (2020). Membrane tension buffering by caveolae: a role in cancer? *Cancer Metastasis Rev.* **39**, 505-517. doi:10.1007/s10555-020-09899-2
Sinha, B., Köster, D., Ruez, R., Gonnord, P., Bastiani, M., Abankwa, D., Stan, R. V., Butler-Browne, G., Vedie, B., Johannes, L. et al. (2011). Cells respond to mechanical stress by rapid disassembly of caveolae. *Cell* **144**, 402-413. doi:10.1016/j.cell.2010.12.031
Smith, S. B., Cui, Y. and Bustamante, C. (2003). Optical-trap force transducer that operates by direct measurement of light momentum. *Methods Enzymol.* **361**, 134-162. doi:10.1016/S0076-6879(03)61009-8
Sparkes, I. (2018). Lessons from optical tweezers: quantifying organelle interactions, dynamics and modelling subcellular events. *Curr. Opin. Plant Biol.* **46**, 55-61. doi:10.1016/j.pbi.2018.07.010
Staunton, J. R., Vieira, W., Fung, K. L., Lake, R., Devine, A. and Tanner, K. (2016). Mechanical properties of the tumor stromal microenvironment probed In Vitro and Ex Vivo by in situ-calibrated optical trap-based active microrheology. *Cell. Mol. Bioeng.* **9**, 398-417. doi:10.1007/s12195-016-0460-9
Staunton, J. R., Blehm, B., Devine, A. and Tanner, K. (2017). In situ calibration of position detection in an optical trap for active microrheology in viscous materials. *Opt. Express* **25**, 1746. doi:10.1364/OE.25.001746
Staunton, J. R., So, W. Y., Paul, C. D. and Tanner, K. (2019). High-frequency microrheology in 3D reveals mismatch between cytoskeletal and extracellular matrix mechanics. *Proc. Natl. Acad. Sci. U. S. A.* **116**, 14448-14455. doi:10.1073/pnas.1814271116
Sudhakar, S., Kazem, M., Tobias, A., Jachowski, J., Bugiel, M., Jannasch, A. and Schäffer, E. (2021). Germanium nanospheres for ultraresolution picotensiometry of kinesin motors. *Science.* **371**, eabd9944. doi:10.1126/science.abd9944
Syrchina, M. S., Shakhov, A. M., Aybush, A. V., Zalessky, A. D. and Nadtochenko, V. A. (2020). Revealing nucleoplasm mechanics by optical trapping and Brownian motion of nucleolus within mouse GV-oocytes in vivo. *J. Phys. Conf. Ser.* **1695**, 012052. doi:10.1088/1742-6596/1695/1/012052
Tassieri, M. (2019). Microrheology with optical tweezers: peaks & troughs. *Curr. Opin. Colloid Interface Sci.* **43**, 39-51. doi:10.1016/j.cocis.2019.02.006
Tassieri, M., Laurati, M., Curtis, D. J., Auhl, D. W., Coppola, S., Scalfati, A., Hawkins, K., Williams, P. R. and Cooper, J. M. (2016). i-Rheo: Measuring the materials' linear viscoelastic properties "in a step " !. *J. Rheol. (N. Y. N. Y).* **60**, 649-660. doi:10.1122/1.4953443
Taylor, M. A., Waleed, M., Stilgoe, A. B., Rubinsztein-Dunlop, H. and Bowen, W. P. (2015). Enhanced optical trapping via structured scattering. *Nat. Photonics* **9**, 669-673. doi:10.1038/nphoton.2015.160
Tian, A. and Baumgart, T. (2009). Sorting of lipids and proteins in membrane curvature gradients. *Biophys. J.* **96**, 2676-2688. doi:10.1016/j.bpj.2008.11.067
Tolić-Nørrelykke, S. F., Schäffer, E., Howard, J., Pavone, F. S., Jülicher, F. and Flyvbjerg, H. (2006). Calibration of optical tweezers with positional detection in the back focal plane. *Rev. Sci. Instrum.* **77**, 103101. doi:10.1063/1.2356852
Turlier, H., Fedosov, D. A., Audoly, B., Auth, T., Gov, N. S., Sykes, C., Joanny, J. F., Gompper, G. and Betz, T. (2016). Equilibrium physics breakdown reveals the active nature of red blood cell flickering. *Nat. Phys.* **12**, 513-519. doi:10.1038/nphys3621
Valentine, M. T., Guydosh, N. R., Gutiérrez-Medina, B., Fehr, A. N., Andreasson, J. O. and Block, S. M. (2008). Precision steering of an optical trap by electro-optic deflection. *Opt. Lett.* **33**, 599. doi:10.1364/OL.33.000599
Valentino, F., Sens, P., Lemière, J., Allard, A., Betz, T., Campillo, C. and Sykes, C. (2016). Fluctuations of a membrane nanotube revealed by high-resolution force measurements. *Soft Mat.* **12**, 9429-9435. doi:10.1039/C6SM02117D
Venturini, V., Pezzano, F., Castro, F. C., Häkkinen, H. M., Jiménez-Delgado, S., Colomer-Rosell, M., Marro, M., Tolosa-Ramon, Q., Paz-López, S., Valverde, M. A. et al. (2020). The nucleus measures shape changes for cellular proprioception to control dynamic cell behavior. *Science (80-.).* **370**, eaba2644. doi:10.1126/science.aba2644
Verdier, C. (2003). Rheological properties of living materials. From cells to tissues. *J. Theor. Med.* **5**, 67-91. doi:10.1080/10273360410001678083
Vermeulen, K. C., Van Mameren, J., Stienen, G. J. M., Peterman, E. J. G., Wuite, G. J. L. and Schmidt, C. F. (2006). Calibrating bead displacements in optical tweezers using acousto-optic deflectors. *Rev. Sci. Instrum.* **77**, 013704. doi:10.1063/1.2165568
Visscher, K., Gross, S. P. and Block, S. M. (1996). Construction of multiple-beam optical traps with nanometer-resolution position sensing. *IEEE J. Sel. Top. Quantum Electron.* **2**, 1066-1076. doi:10.1109/2944.577338
White, R. R., Lin, C., Leaves, I., Castro, I. G., Metz, J., Bateman, B. C., Botchway, S. W., Ward, A. D., Ashwin, P. and Sparkes, I. (2020). Miro2 tethers the ER to mitochondria to promote mitochondrial fusion in tobacco leaf epidermal cells. *Commun. Biol.* **3**, 161. doi:10.1038/s42003-020-0872-x
Woody, M. S., Capitanio, M., Ostap, E. M. and Goldman, Y. E. (2018). Electro-optic deflectors deliver advantages over acousto-optical deflectors in a high resolution, ultra-fast force-clamp optical trap. *Opt. Express* **26**, 11181. doi:10.1364/OE.26.011181

Wu, P. H., Aroush, D. R.-B., Asnacios, A., Chen, W. C., Dokukin, M. E., Doss, B. L., Durand-Smet, P., Ekpenyong, A., Guck, J., Guz, N. V. et al. (2018). A comparison of methods to assess cell mechanical properties. *Nat. Methods* **15**, 491-498. doi:10.1038/s41592-018-0015-1

Wullkopf, L., West, A. K. V., Leijnse, N., Cox, T. R., Madsen, C. D., Oddershede, L. B. and Erler, J. T. (2018). Cancer cells' ability to mechanically adjust to extracellular matrix stiffness correlates with their invasive potential. *Mol. Biol. Cell* **29**, 2378-2385. doi:10.1091/mbc.E18-05-0319

Zhong, M. C., Wei, X.-B., Zhou, J. H., Wang, Z. Q. and Li, Y. M. (2013). Trapping red blood cells in living animals using optical tweezers. *Nat. Commun.* **4**, 1767-1768. doi:10.1038/ncomms2748

Zhong, M.-C., Wang, Z.-Q. and Li, Y.-M. (2017). Aberration compensation for optical trapping of cells within living mice. *Appl. Opt.* **56**, 1972. doi:10.1364/AO.56.001972

Zia, R. N. (2018). Active and passive microrheology: theory and simulation. *Annu. Rev. Fluid Mech.* **50**, 371-405. doi:10.1146/annurev-fluid-122316-044514